# Dynamics of solar large-scale flows

Hideyuki Hotta[1], Yuto Bekki[2], Laurent Gizon[2,3,4*], Quentin Noraz[5,6] and Mark P. Rast[7]

[1]Institute for Space-Earth Environmental Research, Nagoya University, Chikusa-ku, Nagoya, Aichi, 464-8601, Japan.
[2*]Max-Planck-Institut für Sonnensystemforschung, Justus-von-Liebig-Weg 3, Göttingen, 37077, Germany.
[3]Institut für Astrophysik, Georg-August-Universtät Göttingen, Friedrich-Hund-Platz 1, Göttingen, 37077, Germany.
[4]Center for Space Science, NYUAD Institute, New York University Abu Dhabi, Abu Dhabi, UAE.
[5]Rosseland Centre for Solar Physics, University of Oslo, P.O. Box 1029 Blindern, Oslo, NO-0315, Norway.
[6]Institute of Theoretical Astrophysics, University of Oslo, P.O. Box 1029 Blindern, Oslo, NO-0315, Norway.
[7]Department of Astrophysical and Planetary Sciences, Laboratory for Atmospheric and Space Physics, University of Colorado, Boulder, CO 80309, USA.

*Corresponding author. E-mail: gizon@mps.mpg.de;

**Abstract**

The Sun's axisymmetric large-scale flows, differential rotation and meridional circulation, are thought to be maintained by the influence of rotation on the thermal-convective motions in the solar convection zone. These large-scale flows are crucial for maintaining the Sun's global magnetic field. Over the last several decades, our understanding of large-scale motions in the Sun has significantly improved, both through observational and theoretical efforts. Helioseismology has constrained the flow topology in the solar interior, and the growth of supercomputers has enabled simulations that can self-consistently generate large scale flows in rotating spherical convective shells. In this chapter, we review our current understanding of solar convection and the large-scale flows present

in the Sun, including those associated with the recently discovered inertial modes of oscillation. We discuss some issues still outstanding, and provide an outline of future efforts needed to address these.

**Keywords:** convection, differential rotation, meridional flow, helioseismology, numerical simulation

# Contents

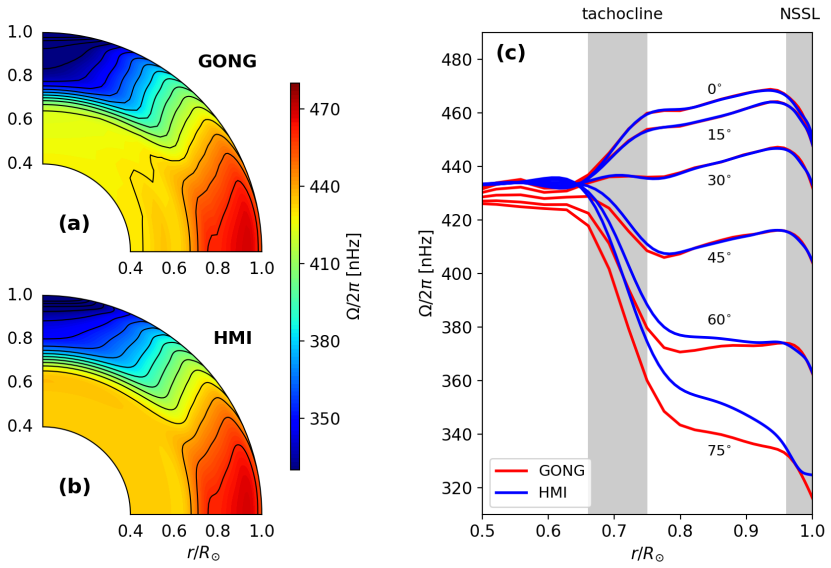


**Fig. 1** Internal profile of the solar differential rotation deduced from global helioseismology. The inversion results obtained from GONG (Howe et al, 2005) and SDO/HMI (Larson and Schou, 2018) mode frequency splittings are shown in panels (a) and (b) respectively. Both results are averaged over time from April 2010 to February 2021. Panel (c) shows the radial differential rotation at selected latitudes. Grey shades denote the layers of strong radial rotational shear called the tachocline and the near-surface shear layer (NSSL).

# 1 Observations of large-scale flows in the Sun

## 1.1 Solar differential rotation and meridional circulation

### Differential rotation

Due to the solar rotation, axisymmetry (about its rotational axis) of the large-scale flows is established to some degree in the Sun's interior. *Differential rotation* is defined as the longitudinal component of the axisymmetric (longitudinally-averaged) flow in the Sun. It arises from the nonlinear interaction of the rotationally-influenced solar magneto-convection (Miesch, 2005). Differential rotation represents a shear in the rotation rate and is thought to play a significant role in the solar dynamo by stretching and amplifying the magnetic field lines (Charbonneau, 2020).

The solar differential rotation profile can be measured by *global helioseismology*, which analyzes small frequency splittings of resonant acoustic oscillations (global standing acoustic modes) (Duvall et al, 1984; Thompson et al, 1996; Schou et al, 1998; Howe et al, 2000). Figure 1 shows the observationally-inferred profile of the internal differential rotation of the Sun (Howe et al, 2005; Larson and Schou, 2018). We summarize striking features of the solar differential rotation as follows:

- The radiative interior rotates almost rigidly.
- In the convection zone, the equator rotates about 30% faster than the poles.
- The transition from uniformly-rotating radiation zone to differentially-rotating convection zone occurs in a thin layer from $0.68R_\odot$ to $0.73R_\odot$. This layer is called the *tachocline*.
- In the bulk of the convection zone ($0.73R_\odot < r < 0.96R_\odot$), the rotation rate is approximately constant in radius and only dependent on latitude.
- In a shallow surface layer ($r \gtrsim 0.96R_\odot$), the rotation rate decreases by about 5% at all latitudes. This layer is called the *near surface shear layer*.
- The contours of constant angular velocity are significantly inclined with respect to the rotational axis. In other words, the differential rotation does not follow the Taylor-Proudmann's theorem.

These observational facts need to be explained by theoretical and numerical models of rotating solar magneto-convection.

### Meridional circulation

*Meridional circulation* represents radial and latitudinal components of the large-scale axisymmetric flow in the Sun, i.e., a poloidal flow in a meridional plane which is perpendicular to the solar rotational axis. Meridional circulation, as well as the differential rotation, is believed to play a significant role in the solar dynamo by advecting the magnetic flux in both radial and latitudinal directions (e.g., Charbonneau, 2020).

The meridional circulation is much weaker than the differential rotation (two orders of magnitudes smaller in flow amplitude) and therefore is extremely difficult to measure. Near the solar surface, the meridional flow is poleward in both hemispheres with typical amplitudes of $\sim 10 - 20$ m s$^{-1}$. This was first measured by Duvall (1979) using Doppler measurements and then robustly confirmed in follow-up studies by a variety of methods (e.g., Patron et al, 1995; Giles et al, 1997; Hathaway, 1996; Braun and Fan, 1998; Haber et al, 2002; Ulrich, 2010; Basu and Antia, 2010).

Local helioseismology can extend these measurements into the deeper convection zone (e.g., Gizon and Birch, 2005). In particular, time-distance helioseismology, in which the cross-covariance of the Doppler signals between the two distant points at the surface are computed to estimate travel times of the acoustic waves (e.g., Duvall et al, 1993; Giles et al, 1997), has been extensively employed. Giles (2000) was the first to apply this method to infer the deep meridional flow pattern. However, this is an extremely difficult measurement to make, because the deeper meridional circulation is very weak ($\sim 3-5$ m s$^{-1}$) and the sensitivity of the method also decreases with depth, leading to overall poor signal-to-noise. Furthermore, for accurate measurements it is critically important to properly deal with systematics such as center-to-limb effects (Duvall and Hanasoge, 2009; Zhao et al, 2012), corrections for $B$ and

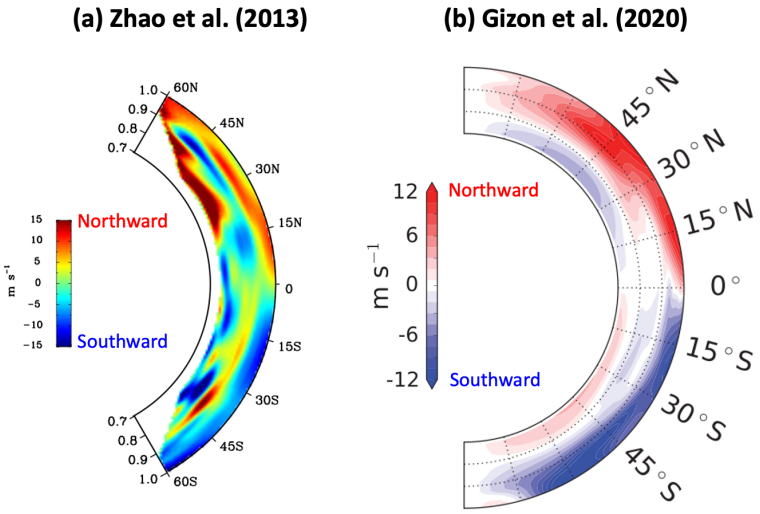


**Fig. 2** Latitudinal component of the meridional flow inferred by time-distance local helioseismology. The red and blue shades correspond to the northward and southward directions respectively. (a) The result obtained by Zhao et al (2013) using SDO/HMI data (2010–2012). (b) The result obtained by Gizon et al (2020a) using GONG data (2008–2019).

$P$-angles (Hathaway and Rightmire, 2010; Liang et al, 2017), and the influence of active region flows (Gizon, 2004; González Hernández et al, 2008). These systematic errors can dominate as the true meridional-circulation signal, depending on the choice of instrument, duration of measurements, and the analysis method (see Hanasoge, 2022, for more details). The importance of these systematic errors has only recently been fully recognized.

Current measurements of the solar meridional circulation are somewhat contradictory. Using travel time measurements obtained from the first 2-years data from SDO/HMI, Zhao et al (2013) detected the equatorward flow in the middle convection zone ($0.82R_\odot - 0.91R_\odot$) and the poleward flow below $0.82R_\odot$, suggesting a *double-cell* structure in radius (Fig. 2a). The similar result was later obtained by Chen and Zhao (2017) who used the 7-years data from HMI in which the active regions were masked out to minimize the contamination from magnetic fields. Note that the mass conservation was not explicitly used as a physical constraint in these analyses. Under the constraint of mass conservation, Rajaguru and Antia (2015), using 4-years of HMI data, found that the meridional circulation is largely *single-cell* in each hemisphere with the equatorial return flow near the base of the convection zone (below $0.77R_\odot$). A similar result was reported by Mandal et al (2018). We note, however, that neither Rajaguru and Antia (2015) nor Mandal et al (2018) removed effects from active region flows in their analysis. These can corrupt the meridional flow measurements (Liang and Chou, 2015)

The inferred meridional flow pattern also depends on the data employed. Jackiewicz et al (2015) have analyzed 2-years of GONG data and detected a

shallow return flow above $0.9R_\odot$ in agreement with the results of Zhao et al (2013) but without a significant pole-ward flow in the deeper convection zone. The similar result was reported by Böning et al (2017), also using GONG data. Liang et al (2018) have examined the instrumental systematics by merging the SOHO/MDI and SDO/HMI data sets. They found a significant offset in the travel times between MDI and HMI measurements.

Recently, Gizon et al (2020a) carried out comprehensive measurements of the solar meridional circulation using all available data sets from GONG, SOHO/MDI, and SDO/HMI that complementally cover the solar cycles 23 and 24. Taking into account all the recognized systematic effects and the constraint of mass conservation, the measured travel times show a good agreement between GONG and MDI. However, a travel time offset is still apparent in the HMI data, as earlier reported by Liang et al (2018). The inverted meridional flows during the cycle 23 (from MDI/GONG data) and cycle 24 (from GONG data) show a clear single-cell pattern in each hemisphere, as shown in Fig. 2b. The yet-unexplained anomaly found in the HMI measurements lead to a strikingly different meridional flow pattern between the northern and southern hemispheres in cycle 24 (Braun et al, 2021).

Unfortunately, no consensus has yet been reached within the community regarding the detailed structure of the meridional circulation in the deep solar interior. Stejko et al (2021) have carried out a forward modelling of travel times using the ray-path approximation, and found that the measured travel times by Gizon et al (2020a) (from GONG/MDI data sets) can be explained by both single-cell and double-cell structures. Still, caution is needed as, in the forward models, travel times are strikingly sensitive to the complex time-varying near-surface flows (Liang et al, 2018). Observational determination of the solar meridional circulation is crucial for, not only constraining solar dynamo models (e.g., Hazra et al, 2014), but also for properly understanding the angular momentum flux balance in the Sun's convection zone (e.g., Featherstone and Miesch, 2015).

## 1.2 Solar convective flows

Convection on the Sun occurs over a wide range of spatial scales, and while the spectrum is continuous, apparent characteristic scales are commonly cited: granulation, mesogranulation, supergranulation, and giant cells. Granulation (Herschel, 1801) is readily apparent in high-resolution images of the solar photosphere, as a pattern of bright upflowing regions separated by darker downflowing lanes. The characteristic upflow cells have diameters of $\sim$ 1000 km, lifetimes of about 0.2 hr, and vertical flow speeds of $\sim$ 1 km/s. The upflow velocity often peaks near the granular boundaries (e.g., Nesis et al, 1992; Rast, 1995; Hirzberger, 2002; Nordlund et al, 2009; Falco et al, 2017, and reference therein). These properties reflect the compressible flow dynamics of a strongly cooled radiative boundary layer, with observations confirming the convective nature of the flow via measurement of the correlation between the vertical velocity and plasma temperature (e.g., Canfield and Mehltretter,

1973). Granulation is well observed and robustly modeled (se e.g., Nordlund et al, 2009), even in quite shallow domains, by codes that capture the rapid change in radiative opacity in the solar photosphere and implement an open lower boundary condition to minimize bottom-up influences on the top-down dynamics of the radiative boundary layer.

Mesogranulation (November et al, 1981), on the other hand, is observationally elusive. With a reported length scale of about $5-10$ Mm, $\sim 60$ m/s vertical flow speeds, and $\sim 2-3$ hr lifetime, its identification as a convective feature is still debated. Most recent studies suggest that no distinct mesogranular scale is present in the broad range of convective scales observed (e.g., Rincon and Rieutord, 2018, and references therein). One possibility is that there is weak advective self-organization of the granular flows, a process first proposed in the context of supergranulation (Rieutord et al, 2000; Rast, 2003) but likely more relevant on mesogranular scales (Cattaneo et al, 2001; Berrilli et al, 2005; Leitzinger et al, 2005; Duvall and Birch, 2010). However, the absence of a mesogranular scale in the clustering of magnetic elements in high resolution magnetograms suggests that this mechanism too leads to a continuous exponential distribution of scales between 2 and 10 Mm, with no distinctive characteristic peak (Berrilli et al, 2013).

Supergranulation (Hart, 1954; Leighton et al, 1962) is the largest likely-convective scale of motion readily visible in the solar photosphere. It is observed directly in spectral Doppler shifts away from disk center (due to horizontal motions) and is traced by network magnetic elements which are prominent in magnetograms and in emission in low chromospheric lines such as Ca II K. There is good correlation between Ca II K emission and magnetic flux density (Ortiz and Rast, 2005, and references therein). Supergranular cells have diameter of $\sim 30$ Mm, horizontal flow velocities of $\sim 100$ m/s, and lifetimes of $\sim 20$ hr. After the intensity contributions of the small scale magnetic field elements has been removed, they show an average continuum intensity contrast across the cells of about 0.1%, corresponding to about one degree Kelvin in brightness temperature (Goldbaum et al, 2009).

The origin of the supergranular motions has been widely debated (see Rincon and Rieutord, 2018, and references therein). It has recently been proposed that the scale of supergranulation reflects not a selected convective scale, but is instead defined by the scale above which convective power declines (Lord et al, 2014; Cossette and Rast, 2016). This interpretation, and the reasons underlying the power reduction, links the well observed phenomenon of supergranulation to the convective conundrum, an outstanding discrepancy between models and observations (see this section below, and Sections 2.2 and 3.1). We note that the early suggestion that helium ionization plays a role in determining the mesogranular and supergranular scales (Leighton et al, 1962; Simon and Leighton, 1964) is not supported by numerical simulations or simplified models base on them (Rast and Toomre, 1993; Lord et al, 2014). Additionally, the presence of the network magnetic elements themselves (Crouch et al, 2007; Thibault et al, 2012) or the enhanced radiative loses through them (Rast, 2003)

do not seem to play a role in scale selection role (Lord, 2014). Finally, it is important to note that supergranulation shows peculiar unexplained wave-like properties (Gizon et al, 2003; Schou, 2003; Langfellner et al, 2018).

In contrast with supergranulation, which is readily observed but not captured by any local-area or global spherical-shell simulation, solar giant cells (Simon and Weiss, 1968), motions on the scale of the solar convection zone depth ($\sim$ 200 Mm), dominate global spherical-shell simulations but are very difficult to observe (Hathaway et al, 2013; Hathaway and Upton, 2021, and references therein). If, in the Sun, giant-cells had the amplitude they do in simulations, they would be easily observed in the solar photosphere. This is the simplest manifestation of the convective conundrum: that supergranulation, rather than giant-cell scale motions, are the largest readily observed motions in the solar photosphere. The implication for solar differential rotation is fundamental. The enhanced amplitude of the large-scale convective motions in global numerical simulations tend to place those simulations in a Rossby-number regime that favors anti-solar differential rotation profiles. Higher rotation rates than those observed are necessary to achieved solar like profiles (O'Mara et al, 2016, and references therein).

These issues are critical to our understanding of large scale motions on the Sun. As can be seen in Figure 3 (from Hathaway et al (2015)), only two of the components described above are evident as distinct features in the observed spectrum of motions in the solar photosphere. Granulation is responsible for the most pronounced peak at high spherical-harmonic degree and supergranulation for the smaller peak near spherical-harmonic degree 120. Added to the plot are vertical fiducial lines indicating the approximate scale of supergranulation and giant cells. Additionally, a *blue dotted* line has been added to schematically indicate the monotonic increase of power to low wavenumbers seen in all numerical simulations up until the most recent of Hotta and Kusano (2021). In the Hotta and Kusano (2021) simulations in the power rolls over at spherical-harmonic degree $\sim$ 10. It is the discrepancy in low spatial-frequency power between simulations and observations that has come to be known as the convective conundrum.

It is important to note that the spectrum plotted in Figure 3 is a composite, with vertical velocities dominating at high spatial wavenumbers (granular scales) and horizontal motions most important at supergranular scales. The vertical velocity contribution decreases from the granular peak towards lower wavenumbers, with horizontal velocity contribution increasing to spherical-harmonic degree $\sim$ 120 before rolling over beyond that. The supergranular peak results from this decrease in the power beyond spherical-harmonic degree $\sim$ 120. Thus, with respect to photospheric flow observations, the convective conundrum refers to the scale and amplitude of the horizontal-flows in the photosphere. No global-spherical-shell or local-area simulation of solar convection yet captures the supergranular scale maximum in photospheric horizontal-flow power.

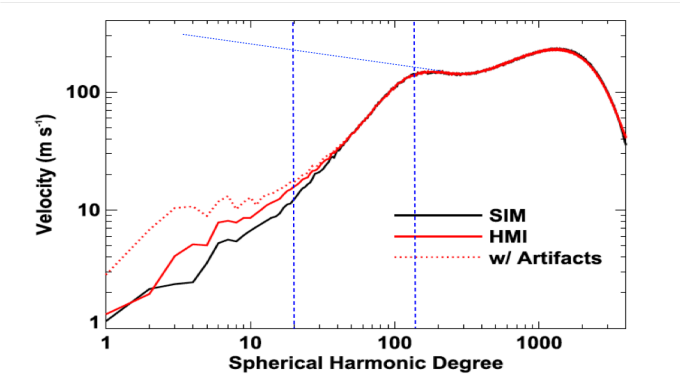


**Fig. 3** Solar Doppler velocity spectrum as determined from Helioseismic and Magnetic Imager (HMI) observations (red curves, with and without removal of image artifacts), along with a random-phase synthetic spectrum (black curve, Hathaway et al, 2000). Vertical blue dashed fiducial lines have been added indicating the approximate scale of supergranulation and giant-cells. The blue dotted line approximately over-plots the spectrum seen in numerical simultions. Figure without additional dashed and dotted blue lines courtesy of Hathaway et al (2015).

## 1.3 Solar inertial modes

Inertial waves are travelling waves in a rotating fluid (Greenspan et al, 1968). Their restoring force is the Coriolis force. In a rotating sphere, the frequencies of inertial modes are limited to a range of $|\omega| < 2\Omega_0$ in the co-rotating frame, where $\Omega_0$ denotes the rotational angular frequency. The traditional Rossby modes (or r modes) correspond to a variety of inertial modes that have quasi-toroidal motions. Although these modes have been expected to exist in the Sun and stars since the late 1970's (e.g., Papaloizou and Pringle, 1978; Saio, 1982; Unno et al, 1989), they were not observed on the Sun until very recently. Inertial modes on the Sun have very long oscillation periods (of the order of months) and very small velocity amplitudes (of the order of 1 m s$^{-1}$). Therefore, long-term and high-precision observations of horizontal flows over many years are required to detect them.

Löptien et al (2018) discovered the solar equatorial Rossby modes using both a granulation-tracking method and ring-diagram analysis applied to six years of SDO/HMI data. These Rossby modes are retrograde-propagating waves of radial vorticity. Löptien et al (2018) found the excess power in the radial vorticity along the dispersion relation of the sectoral Rossby modes, $\omega = -2\Omega_{\rm eq}/(m+1)$, for azimuthal orders $3 \leq m \leq 15$. In this formula, $\Omega_{\rm eq}$ is the equatorial rotation rate of the Sun at the surface. For $m \gtrsim 5$, the latitudinal eigenfunctions of the equatorial Rossby modes significantly deviate from the sectoral spherical harmonics: the radial vorticity peaks at the equator but changes sign at middle latitudes. The detection of solar equatorial Rossby modes has been confirmed in follow-up studies using various other observational datasets and methods (Liang et al, 2019; Proxauf et al, 2020; Mandal and Hanasoge, 2020; Hanson et al, 2020; Hathaway and Upton, 2021).

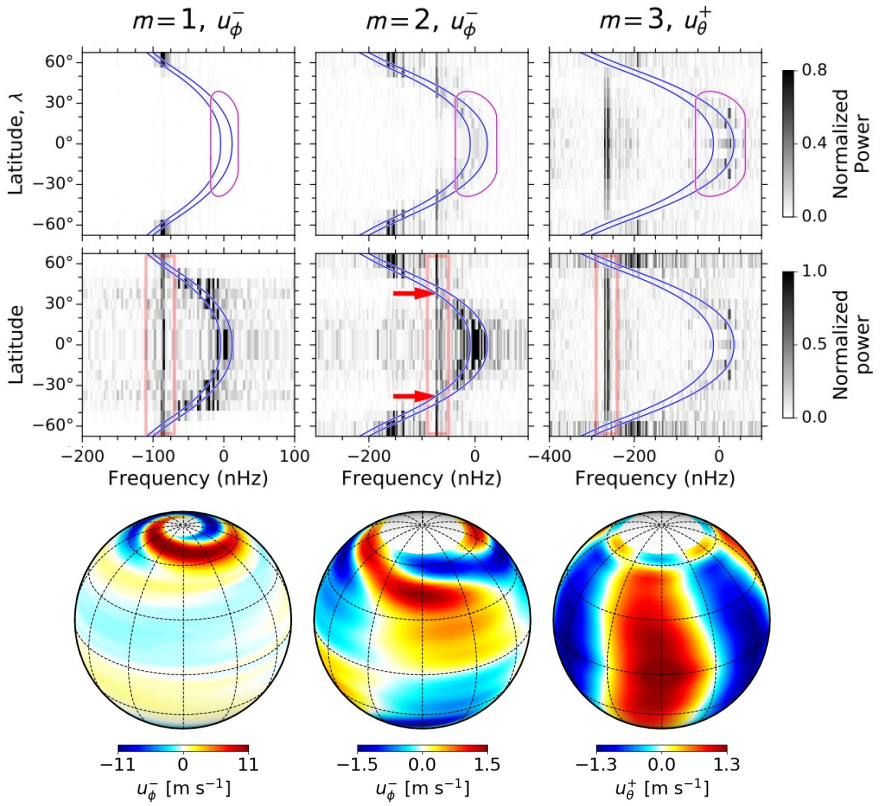


**Fig. 4** Observational power spectra in the Carrington frame and eigenfunctions of three selected inertial modes of the Sun. *Top row*: Power spectra of the longitudinal component of velocity $u_\phi$ for $m = 1$ (left column) and $m = 2$ (middle column), and power spectrum of the colatitudinal component of velocity $u_\theta$ for $m = 3$. The blue curves show the differential rotation rate at $r = 0.96R_\odot$ and $R_\odot$. The purple contour indicates the region affected by active-region flows. *Middle row*: The same power spectra but normalized at each latitude by their average value over the frequency range between the orange bars. Excess power is seen at a specific frequency at all latitudes in each of the three cases. The red arrows point to critical latitudes at the surface for the case $m = 2$. *Bottom row*: Observed horizontal velocity eigenfunctions at the surface for the $m = 1$ high-latitude mode, the $m = 2$ critical-latitude mode, and the $m = 3$ equatorial Rossby mode. The figures are taken from Gizon et al (2021).

The observed equatorial Rossby modes exist only at very large scales with $m \leq m_{\rm crit} = 15$. Löptien et al (2018) speculated that this critical azimuthal order $m_{\rm crit}$ might reflect the Rhines scale $l_{\rm rhines} = \sqrt{R_\odot v_{\rm c}/\Omega_\odot}$ above which rotation strongly affects turbulent convection (Rhines, 1975). Assuming $m_{\rm crit} \approx R_\odot/l_{\rm rhines}$, a typical speed of turbulent convection can be roughly estimated as $v_{\rm c} \approx 9$ m s$^{-1}$, which is about one order magnitude smaller than the typical mixing-length estimate (Böhm-Vitense, 1958; Stix, 2002). This may add another evidence to the solar convective conundrum (see Sections 2.2 and 3.1 below).

Recently, Gizon et al (2021) analyzed more than 10 years of data from both SDO/HMI and GONG in search for additional quasi-toroidal inertial modes with $1 \leq m \leq 10$. With the help of a 2.5D linear eigenmode analysis (Bekki et al, 2022b), they observed and identified not only equatorial Rossby modes, but also modes at middle and high latitudes. The observational power spectra and the measured eigenfunctions of three selected inertial modes with $m = 1, 2$, and 3 are shown in Fig. 4. These modes owe their existence to the solar latitudinal differential rotation (see Gizon et al, 2020b, for a discussion in the $\beta$ plane). For some inertial modes, there exists latitudes at which the phase speed is equal the local differential rotation speed; such latitudes are called critical latitudes (see Fig. 4, middle column). The $m = 1$ high-latitude mode has a large amplitude ($v_\phi \approx 10 - 20$ m s$^{-1}$) above $\sim 50^\circ$ and its surface eigenfunction exhibits a spiral pattern in the polar regions. The horizontal flow associated with the $m = 1$ high-latitude mode was first observed by Hathaway et al (2013), but misidentified at the time as giant cell convection. A linear model suggests that this $m = 1$ high-latitude mode is self-excited when a large enough latitudinal entropy gradient exists in the convection zone (Bekki et al, 2022b).

More recently, Hanson et al (2022) reported the detection of another class of inertial modes with north-south anti-symmetric radial vorticity across the equator. These modes propagate in a retrograde direction with the phase speed roughly three times faster than the that of the equatorial Rossby modes. Compared with the equatorial Rossby modes and the high-latitude modes reported in Gizon et al (2021), these so-called *high-frequency retrograde* modes have lower velocity amplitudes and are thus much harder to distinguish from the background noise in the power spectra. According to simplified linear eigenmode calculations of a uniformly-rotating Sun (Triana et al, 2022; Bhattacharya and Hanasoge, 2022), these modes are not quasi-toroidal, i.e., substantial radial motions are involved.

Though it remains unclear how important the solar inertial modes are to the overall convection zone dynamics, it is expected that they might play an important diagnostic role. Gizon et al (2021) and Bekki et al (2022b) have shown that the properties of some inertial modes (i.e., frequencies, linewidths, and surface eigenfunctions) are sensitive to the turbulent viscous diffusivity $\nu_{\rm t}$ and to the superadiabaticity $\delta$ of the convection zone. Gizon et al (2021) inferred that, on average, $\nu_{\rm t} \leq 10^{12}$ cm$^2$ s$^{-1}$ and $\delta < 2 \times 10^{-7}$. These values are an order of magnitude smaller than the theoretical estimates from the local mixing length model (Christensen-Dalsgaard et al, 1996; Muñoz-Jaramillo et al, 2011). It is noteworthy that both of these parameters cannot be constrained by conventional p-mode helioseismology, and are important in discussions of the convective conundrum (Sections 2.2 and 3.1 below) and the solar dynamo. The amplitudes of the linearly-stable modes might provide additional constraints on the turbulent viscosity (Philidet and Gizon, 2023). On the other hand, to better understand the amplitudes of the linearly-unstable

inertial modes, nonlinear numerical simulations will be required (Bekki et al, 2022a; Bekki and Cameron, 2023).

## 1.4 Observations of large-scale flows on solar-type stars

Even if we cannot directly observe the surface of other stars in the vast majority of cases, it is possible to find traces of surface vibrations in their light curve, and thus to probe indirectly the interior of these stars. This is known as *asteroseismology* (see García and Ballot (2019) for a recent review). Although the application of asteroseismic techniques remains difficult, with application primarily to bright stars after long monitoring, it has become possible in the last 10 years to probe the deep interior of some evolved stars, first for red giants (Beck et al, 2012; Deheuvels et al, 2012), and more recently for subgiants (Deheuvels et al, 2020).

Radial profiles of differential rotation have also recently been reconstructed by Benomar et al (2018) for main-sequence solar-type stars presenting strong seismic signal. These authors report clear detection of a solar-like differential rotation profile (equator faster than the poles) on 13 stars with notably stronger latitudinal contrast than the Sun (averaging twice the solar value). Subsequent researchers (Bazot et al, 2019) have reported contrasts closer to the solar within two solar analogs 16 Cyg A and B. The difference in latitudinal contrast $\Delta\Omega$ may reflect to the mean rotation rate of the stars, with the majority of stars in Benomar et al (2018) study rotating faster than the Sun. In this context, it is important to understand the trends of the differential rotation as a function of stellar parameters, such as the stellare mass $M_*$, the rotation rate $\Omega_*$, composition and age.

It has been observed that the stellar differential rotational contrast has power law dependence on mean rotation rate, $\Delta\Omega \propto \Omega_*^n$. Figure 3 of Barnes et al (2005) summarizes the different studies that have been undertaken. Long-term monitoring of photometric modulations point toward a weak rotational dependence, $n = 0.24$ (Henry et al, 1995), while similar observations in H & K bands of Ca II emission suggest a significantly higher value, $n = 0.7$ (Donahue et al, 1996). These have been consolidated by careful spectral analysis (Reiners and Schmitt, 2003) to yield a power law index of $n = 0.66$[1]. Barnes et al (2005) concludes that all the data together suggests an index of $n = 0.15$, but also shows that this index is very sensitive to the spectral diversity of the target sample of targets considered (see also Reiners and Schmitt, 2003). This is supported by Reinhold et al (2013) who find a value of $n = 0.3$ for cool stars and Balona and Abedigamba (2016) who arrive at $n = 0.2$ for G-stars. Asteroseismic studies tend to find values for $n$ between 0.3 and 0.45, and underline its sensitivity to the effective temperature $T_{\rm eff}$ range of the stars considered (see Reinhold and Gizon (2015) and references therein).

[1] It is important to note that these measurements give very few indications about the latitude of the active region responsible for the modulation. The measurements capture the range of latitudes explored by active regions during the stellar activity cycle, and thus yield only lower limits to the latitudinal contrast.

The dependence of the latitudinal contrast $\Delta\Omega$ on spectral type appears to also be true of fast main-sequence rotators. Collier Cameron (2007) study fast M, K, G, and F main-sequence rotators and report a strong $\Delta\Omega \propto T_{\rm eff}^{8.6}$ dependence on the effective temperature, consistent with Barnes et al (2005). Large error bars are associated with the hottest spectral types, however the models of Kueker and Ruediger (2011) tend to confirm a strong dependence (see Reinhold and Gizon (2015) for detailed discussion).

To take into account both rotational and spectral aspects, Saar (2010) proposed to study the global shear $\Delta\Omega$ as a function of the stellar Rossby number $Ro_{\rm s} = \tau_{\rm c}/\Omega_*$ (see Appendix B of Brun et al 2017 for a discussion of the definition). Indeed, it is possible to parameterize the convective turnover time $\tau_{\rm c}$ as a function of $T_{\rm eff}$ (Cranmer and Saar, 2011), which can then be taken into account in these dependencies. In particular, he finds that $\Delta\Omega \propto Ro_{\rm s}^{-1}$ for unsaturated rotators ($\Omega \leq 12\Omega_\odot$), pointing then toward $n = 1$ when fixing $T_{\rm eff}$ and the composition (Noraz et al, 2022a).

Finally, if the impact of the star composition was not the main focus initially, recent observational studies have started to investigate the impact of the metallicity, for instance with the solar analog HD 173701 studied by (Karoff et al, 2018). Its parameters are indeed close to the solar ones, while having a significantly higher metallicity ([Fe/H]$= 0.3 \pm 0.1$). Using different methods previously mentioned, the authors report a solar-like differential rotation (fast equator) with a latitudinal contrast twice the solar one. Monitoring of its chromospheric and photometric emissions also show a cyclic activity shorter than the one observed on the Sun ($P_{\rm cyc} = 7.4$ agains 11 years), while having a higher amplitude of variation, which underlines the entanglement between composition, large-scale flows and magnetism (see Brun and Browning (2017) for a review).

To summarize, differential rotation is a characteristic quantity of stellar convective envelopes. Apart from the Sun, the exact quantification of the surface rotational contrast remains difficult because it requires a high degree of precision of the instruments used and long acquisition periods for the different targets. New observations by the upcoming PLATO mission should allow major advances in this direction (Rauer et al, 2014). In the meantime, theoretical modeling of these flows appears to be crucial for the understanding and support of these observations, and to guide those to come.

# 2 Models of large-scale flows

Large-scale flows in the Sun are generated and maintained by thermal convection. In this section we briefly summarize the current theoretical understanding of how that occurs.

## 2.1 Mixing length theory and energy budget

Mixing-length theory (MLT; Böhm-Vitense, 1958) remains a remarkably useful way to describe the mean energy transport by convection even when the actual

dynamics are far from localize eddy motions. In the mixing length formulation, we can relate energy flux to the convective velocity and the stratification through a parameter called the mixing-length parameter $\alpha_{\rm MLT} = L_{\rm MLT}/H_p$, where $L_{\rm MLT}$ and $H_p = -\left(d\log p/dr\right)^{-1}$ are the mixing length and the pressure scale height in the convecting fluid. The mixing length, $\alpha_{\rm MLT}$ is an $\mathcal{O}(1)$ parameter which mainly affects the stellar radius (Demarque and Percy, 1964) when used in a stellar stucture model. Here we take $\alpha_{\rm MLT} = 1$ (i.e., $L_{\rm MLT} = H_p$) for the simplest mixing-length formulation. The typical temperature perturbation in the convection $\Delta T$ is then evaluated as:

$$\begin{aligned}\Delta T &= \left[\left(\frac{dT}{dr}\right)_{\rm ad} - \frac{dT}{dr}\right] L_{\rm MLT} = T\left[\left(\frac{d\log T}{d\log p}\right)_{\rm ad} - \left(\frac{d\log T}{d\log p}\right)\right] \\ &= -T\delta\ , \end{aligned} \tag{1}$$

where $\delta = (d\log T/d\log p) - (d\log T/d\log p)_{\rm ad}$ is the superadiabaticity, the deviation from the adiabatic stratification. When the speed of sound in the medium is much faster than convection, the sound wave instantaneously relaxes any pressure perturbation $\Delta p$, and the density perturbation $\Delta\rho$ can be estimated from the linearized equation of state as

$$\frac{\Delta\rho}{\rho} = -\frac{\Delta T}{T} = \delta\ . \tag{2}$$

A simplified equation of motion is converted with rough dimensional analysis as

$$\rho\frac{Dv}{Dt} = -\Delta\rho g \rightarrow \frac{v_{\rm c}}{\tau_{\rm c}} = -\frac{\Delta\rho}{\rho}g, \tag{3}$$

where $v_{\rm c}$ is the typical convection velocity. Here we can evaluate the typical time for the convection as $\tau_{\rm c} = H_p/v_{\rm c}$. Then the convection velocity can be written as

$$v_{\rm c}^2 = \delta\frac{p}{\rho} \sim \delta c_{\rm s}^2\ , \tag{4}$$

where $c_{\rm s}$ is the speed of sound. Together, these approximations yield several important approximations for the superadiabaticity:

$$\delta \sim \frac{\Delta T}{T} \sim \frac{\Delta\rho}{\rho} \sim \left(\frac{v_{\rm c}}{c_{\rm s}}\right)^2, \tag{5}$$

While some more careful treatments include additional physical effects, such as variation in the mean molecular weight of the plasma or the fluid drag force, in the practical application of MLT, the relationships captured by Equation 5 change little. What is important is that these relations lead to

a ratio of the kinetic energy $E_{\rm kin}$ to the internal energy $E_{\rm int}$ that scales with superadiabaticity $\delta$:

$$\frac{E_{\rm kin}}{E_{\rm int}} \sim \frac{\rho v_{\rm c}^2/2}{\rho c_{\rm v} T} \sim \left(\frac{v_{\rm c}}{c_{\rm s}}\right)^2 \sim \delta \ . \tag{6}$$

In the convection zone, heat is mainly transported by the convection, with the enthalpy flux given by

$$F_e = \rho c_{\rm p} \Delta T v_{\rm c} \sim \rho v_{\rm c}^3 \ . \tag{7}$$

Normalized by the density and sound speed the flux can thus be written as

$$\frac{F_e}{\rho c_{\rm s}^3} \sim \left(\frac{v_{\rm c}}{c_{\rm s}}\right)^3 \sim \delta^{3/2} \ . \tag{8}$$

Over the depth of the convection zone, with the superadiabaticity taken to $10^{-6}$ and $10^{-1}$ at the base and surface respectively, the convective velocity amplitudes should change by a factor of a few hundred. At the base of the solar convection zone, the flow is subsonic (Mach number $\sim 10^{-3}$) and the internal energy of the fluid is much larger ($10^6$ times larger) than the kinetic energy of the flows. This is true even in the near surface layers where the convective velocities are nearly sonic.

## 2.2 The effect of stratification on observed horizontal convective flow amplitudes

As is clear from the mixing-length calculation above, one of the most important aspect of stellar envelope convection is the steep stratification of the mean state. The solar convection zone is about 210 Mm deep, over which the density changes by a factor of about one million and the pressure by about 800 million. The density scale height in the photosphere is about 150 km, while at the convection zone base it is equal to nearly half the depth. This has profound influence on the convective dynamics.

By mass conservation, only a very small fraction of the upwelling fluid from the deep convection zone makes it into the photosphere. The rest must overturn. Over each scale height, the density decreases by a factor of $1/e$, so that $1-1/e$ of the mass must over turn. Similarly, the downwelling fluid must entrain mass at this rate. For simple assumptions about the flow geometry, this implies a characteristic horizontal flow scale at each depth $d = 4H_\rho$, where $H_\rho$ is the density scale height (Nordlund et al, 2009). Taking this to be the integral (driving) scale of the motions (Stein et al, 2009) allows a simple two component model that can reproduce the observed spectrum of horizontal motions in the solar photosphere (Lord et al, 2014).

For statistically steady motions and small horizontal density gradients compared to the mean vertical stratification, the equation of mass continuity takes

the form

$$\nabla_{\rm h} \cdot \mathbf{u}_h = -\frac{\partial u_z}{\partial z} - \frac{u_z}{H_\rho} \ . \tag{9}$$

This suggest two flow regimes. For $\partial u_z/\partial z \gg u_z/H_\rho$ the motions are nearly divergenceless and for $\partial u_z/\partial z \ll u_z/H_\rho$ the vertical stratification dominates. In these two limits, Equation 9 can be used to determine the horizontal velocity power spectrum given that of the vertical velocity. For small scale motions, high horizontal wavenumbers $k_h$, the motions are nearly isotropic with

$$\widetilde{\mathbf{u}}^*_{\rm h} \cdot \widetilde{\mathbf{u}}_{\rm h} = \widetilde{u}^*_z \widetilde{u}_z \ , \tag{10}$$

where $\widetilde{\mathbf{u}}^*_{\rm h} \cdot \widetilde{\mathbf{u}}_{\rm h}$ is the power spectrum of the horizontal flows and $\widetilde{u}^*_z \widetilde{u}_z$ is that of the vertical flows. For low wavenumber components of the flow, on the other hand, stratification is important and

$$\widetilde{\mathbf{u}}^*_h \cdot \widetilde{\mathbf{u}}_h = \frac{2}{k_h^2 H_\rho^2} \widetilde{u}^*_z \widetilde{u}_z \ . \tag{11}$$

The cross over between these two regimes occurs at the integral scale $4H_\rho$ at each depth. Figure 1 of Lord et al (2014) confirms that this two-component continuity balance determines the relationship between the vertical and horizontal-velocity power spectra in radiative hydrodynamic simulations.

Using this balance, a model of the horizontal motions observed in the solar photosphere can be constructed from the vertical velocity spectrum at each depth. For example, the high-wavenumber vertical-velocity spectrum can be taken to be Kolmogorov above the integral scale $4H_\rho$, with a mixing length approximation to determine the total integrated power. Since no scales larger than that are driven at any given depth, the amplitudes of modes with scales larger than the driving scale at any depth can be determined by their decay with height from the depth at which they were last driven. A potential flow approximation on these scales can be used to model that amplitude decrease with height. With these ingredients, working from the bottom of the convection zone upwards, the power spectrum of the horizontal velocity at each depth can be determined. It matches that seen in three-dimensional radiative hydrodynamic simulations, (Lord et al, 2014). The broader and critical take away from this simplified approach is that the horizontal-velocity spectrum in the photosphere depends on the vertical-velocity flow amplitudes at depth. The larger the horizontal flow scale observed in the photosphere, the deeper it originates. This suggests that the dramatic decrease in the observed horizontal-velocity power above the supergranular scale on the Sun reflects weak convective driving at depth (at depths below $\sim$ 10Mm) and that supergranulation represents the largest buoyantly driven scale of motion (Lord et al, 2014; Cossette and Rast, 2016).

A number of reasons for the low-convective amplitudes at depth are possible, including highly non-local dynamics (maintainence of small scale downflowing plumes generated in the photosphere with little horizontal diffusion) that ensures that the mean stratification of the solar convection zone is closer to adiabatic than numerical models can achieve (Cossette and Rast, 2016; Rast, 2020), this possibly due to the presence of small scale magnetic field (O'Mara et al, 2016; Bekki et al, 2017); subadiabatic stratification in the deep solar convection zone due to internal heating by radiation; reduced convective amplitudes due to the stabilizing influence of rotation in the lower convection zone (Featherstone and Hindman, 2016; Vasil et al, 2021); or a combination of these. Any mechanism that leads to reduced convective amplitudes in the deep layers of the solar convection zone will be reflected in reduced low wavenumber power in the horizontal-flows at the surface.

In radiative hydrodynamic simulations, a factor of $\sim 2.5$ reduction in convective amplitudes below $\sim 10$Mm depth is sufficient to resolve the convective conundrum (Lord et al, 2014). Though such a reduction has not been yet achieved in a first principles model of convection, we note that, by simple mixing-lenght scaling arguements (Equation 5), it is consistent with the reduction in superadiabaticity ($\delta < 2 \times 10^{-7}$) suggested by the Gizon et al (2021) analysis of solar inertial modes.

## 2.3 Gyroscopic pumping and thermal wind balance

Given the convective motions, it is important to understand how, in combination with solar rotation, they generate and maintain large-scale solar differential rotation and meridional circulation. For that purpose, the concepts of gyroscopic pumping and the thermal wind balance are useful (McIntyre, 1999; Miesch et al, 2008; Miesch and Hindman, 2011). We discuss those in this section. In this discussion, for simplicity the magnetic field is ignored, though it may be critical in some cases (Hotta et al, 2022), and notationally, a quantity $Q$ is divided into a mean (longitudinal average) $\langle Q \rangle$ and perturbation $Q'$, i.e., $Q = \langle Q \rangle + Q'$.

Gyroscopic pumping is a reflection of angular momentum conservation. The longitudinally averaged longitudinal equation of motion under the anelastic approximation can be written as

$$\rho_0 \frac{\partial \langle \mathcal{L} \rangle}{\partial t} = -\nabla \cdot \left( \rho_0 \langle \boldsymbol{v}_{\rm m} \mathcal{L} \rangle \right), \tag{12}$$

where $\mathcal{L} = \lambda v_\phi$ and $\boldsymbol{v}_{\rm m} = v_r \boldsymbol{e}_r + v_\theta \boldsymbol{e}_\theta$ are the specific angular momentum and the meridional flow, respectively, with $\lambda = r \sin\theta$ in the spherical geometry $(r, \theta, \phi)$. We also note $\rho_0$ the density background profile (spherical average). The symbols $\boldsymbol{u}$ and $\boldsymbol{v}$ and their components are used to indicate the fluid velocities in the inertial and rotational frames. The flow is then divided into components, as above, $\boldsymbol{v} = \langle \boldsymbol{v} \rangle + \boldsymbol{v}'$ and, assume a steady state $\partial / \partial t = 0$

balance, the equation for gyroscopic pumping can be written

$$\rho_0 \left( \langle \boldsymbol{v}_\mathrm{m} \rangle \cdot \nabla \right) \langle \mathcal{L} \rangle = -\nabla \cdot \left( \rho \lambda \langle \boldsymbol{v}'_\mathrm{m} v'_\phi \rangle \right). \tag{13}$$

While the angular momentum conservation equation (12) determines the temporal evolution of the differential rotation, the gyroscopic pumping balance (Equation 13) mainly determines the meridional flow $\langle \boldsymbol{v}_\mathrm{m} \rangle$ in a steady state. The distribution of the specific angular momentum $\langle \mathcal{L} \rangle$ is mostly cylindrical, i.e., $\partial \langle \mathcal{L} \rangle / \partial z \sim 0$, where $z$ denotes the direction of the rotational axis even if the differential rotation $\langle \Omega \rangle$ has a conical profile, $\partial \langle \Omega \rangle / \partial r \sim 0$. Thus gyroscopic pumping can be rewritten as

$$\rho \langle v_\lambda \rangle \frac{\partial \mathcal{L}}{\partial \lambda} \approx -\nabla \cdot \left( \rho_0 \lambda \langle \boldsymbol{v}'_\mathrm{m} v'_\phi \rangle \right). \tag{14}$$

Since we know that the sign of $\partial \langle \mathcal{L} \rangle / \partial \lambda$ is greater than zero, the sign of the axial turque $\mathcal{T} = -\nabla \cdot \left( \rho_0 \lambda \langle \boldsymbol{v}'_\mathrm{m} v'_\phi \rangle \right)$ directly determines the direction of the meridional flow.

The thermal wind balance equation is derived from the longitudinal vorticity equation,

$$\frac{\partial \langle \omega_\phi \rangle}{\partial t} = \left[ \nabla \times (\boldsymbol{v} \times \boldsymbol{\omega}) \right]_\phi + \lambda \frac{\partial \langle \Omega \rangle^2}{\partial z} - \frac{g}{r c_p} \frac{\partial \langle s \rangle}{\partial \theta}, \tag{15}$$

where $\boldsymbol{\omega} = \nabla \times \boldsymbol{v}$ is the vorticity. This equation is for the evolution of the longitudinal vorticity $\omega_\phi$, in terms of $v_r$ and $v_\theta$, i.e., the meridional flow. In a steady state ($\partial / \partial t = 0$),

$$\lambda \frac{\partial \langle \Omega \rangle^2}{\partial z} = -\left[ \nabla \times (\boldsymbol{v} \times \boldsymbol{\omega}) \right]_\phi + \frac{g}{r c_p} \frac{\partial \langle s \rangle}{\partial \theta}, \tag{16}$$

which reduces to the Taylor-Proudman theorem $\partial \langle \Omega \rangle / \partial z = 0$ when advection $\nabla \times (\boldsymbol{v} \times \boldsymbol{\omega})$ and the latitudinal entropy gradient $\partial \langle s \rangle / \partial \theta$ are ignored. Under the Taylor-Proudman constraint, contour lines of the angular velocity are parallel to the rotational axis. As shown in Fig. 1 the solar differential rotation does not follow this configuration, showing instead the prominent tachocline and the near surface shear layer at its boundaries and a more conical profile in the interior. Thus, either a latitudinal entropy gradient or vorticity stretching (or the magnetic field which we have ignored here) play a role in maintaining its topology.

## 2.4 Governing equations for numerical simulations

Simulating the global scale motions seen on the Sun directly requires simulating the convective motions in a spherical domain over many scale heights. This in turn requires running efficient numerical code on the world's largest

supercomputers. For tractability, a number of approximations must be made during formulation.

The solar convection zone is fully ionized below about 20 Mm, and, for global spherical shell magnetohydrodynamic models of convection below that depth, we can reliably assume the equation of state is close to that of a perfect gas. Simulations of the deep solar convection zone must include rotation along with gravitational stratification, and since the superadiabaticity, i.e., the normalized mean entropy gradient, in the solar convection zone is tiny ($\delta \lesssim 10^{-6}$), solving an entropy equation is preferable to formulations in terms of the total energy or internal energy. The set of equations to be solved (in the invisicd case) can thus be written as

$$\begin{aligned}
\frac{\partial \rho}{\partial t} &= -\nabla \cdot (\rho \boldsymbol{v}) \,, \\
\frac{\partial}{\partial t}(\rho \boldsymbol{v}) &= -\nabla \cdot (\rho \boldsymbol{v}\boldsymbol{v}) - \nabla p + \rho \boldsymbol{g} + \frac{1}{4\pi}(\nabla \times \boldsymbol{B}) \times \boldsymbol{B} + 2\rho (\boldsymbol{v} \times \boldsymbol{\Omega}_0) \,, \\
\rho T \frac{\partial s}{\partial t} &= -\rho T (\boldsymbol{v} \cdot \nabla) s + Q_{\rm rad}, \\
\frac{\partial \boldsymbol{B}}{\partial t} &= \nabla \times (\boldsymbol{v} \times \boldsymbol{B}) \,, \\
s &= c_{\rm v} \log \left( \frac{p}{\rho^\gamma} \right) .
\end{aligned}$$

Moreover, since perturbations in the thermodynamic variables scale with the superadiabicity (Equation 2) a linearized equation of state is appropriate,

$$\frac{s_1}{c_{\rm v}} = \frac{p_1}{p_0} - \gamma \frac{\rho_1}{\rho_0} \,, \tag{17}$$

where subscripts 0 and 1 denote the background and perturbed variables, such that $Q = Q_0 + Q_1$, and we typically assume the hydrostatic balance for the background stratification $\rho_0$, $p_0$, and $T_0$:

$$\frac{dp_0(r)}{dr} = -\rho_0(r) g(r) \,.$$

Pressure gradient and the gravitational forces in the momentum equation are then due to perturbations about this background state,

$$-\nabla p + \rho \boldsymbol{g} \rightarrow -\nabla p_1 + \rho_1 \boldsymbol{g} \,. \tag{18}$$

Due to a large optical depth in the deep convection zone, the diffusion approximation can be used for radiation energy transfer $Q_{\rm rad}$,

$$Q_{\rm rad} = -\kappa_{\rm rad} \nabla T, \tag{19}$$

where $\kappa_{\rm rad}$ is the radiation diffusion coefficient estimated from the local opacity. Finally, due to the large fluid/magnetic Reynolds and Peclet numbers, we can in principle, ignore the viscosity, the magnetic diffusivity, and the thermal conductivity, though in some studies "turbulent' diffusivities are adopted (e.g., Miesch et al, 2000). This latter approach attempts to mimic transport by unresolved small-scale motions not captured by the simulations.

Employing an anelastic approximation is important for deep solar convection simulations. Again, due to the small superadiabaticity of the deep solar convection zone, the speed of sound $c_{\rm s}$ is much faster than the convection velocity $v_{\rm c}$, since $\delta \sim (v_{\rm c}/c_{\rm s})^2$. Explicitly solving for sound waves in the domain severely restricts the CFL condition on the time stepping $\Delta t$, and a huge number of the time steps would be required to evolve the convective motions and larger-scale floes over dynamical time scales. To avoid this difficulty, the anelastic approximation (Gough, 1969) is widely used (Clune et al, 1999), which simplifies the mass-continuity equation,

$$\nabla \cdot (\rho_0 \boldsymbol{v}) = 0 \ , \tag{20}$$

filtering out sound waves by taking the sound speed to be infinite. In the context of MHD, the anelastic approximation eliminates the fast magneto-sonic waves, while preserving the Alfvén waves and the slow magneto-sonic waves.

Other sonic-filter formulations have been developed including the *Lantz-Braginsky-Roberts* (LBR) method, in which a reduce pressure is introduced and interactions between fluctuating pressure and stratification are neglected ( Lantz 1992, Braginsky and Roberts 1995). The LBR method has the advantage of conserving energy well in both unstable convective zones and stable radiative interiors, critical for simulating gravity wave excitation and propagation (Brown et al 2012,Vasil et al 2013).

Recently, a method that has come to be known as the Reduced Speed of Sound Technique (RSST) has also found extensive use. With this, the continuity equation is altered,

$$\frac{\partial \rho_1}{\partial t} = -\frac{1}{\xi^2} \nabla \cdot (\rho \boldsymbol{v}) \ , \tag{21}$$

so that the effective speed of sound is sound is reduced by a factor of $\xi$ (Rempel, 2005; Hotta et al, 2012). An advantage of the RSST method is that it does not requires global communications in a parallel computing environment, in contrast to the anelastic approximation which requires frequent global communication to solve the elliptic equation (20). Thus, the RSST is thus very useful when solving the MHD equations in large domains with massively parallel supercomputers. Additionally, an inhomogeneous $\xi$ can be employed, taking $\xi$ large in the deep layers where the sound speed is fast and $\xi = 1$ in the near-surface layer where the anelastic approximation is not valid. This enables simulation over a continuous domain that cover the whole convection zone (Hotta et al, 2019).

## 2.5 Modeling of the solar large-scale flows

The last fifty years have brought tremendous advances in the simulation of solar and stellar convection and our understanding of the global flows that result in rotating domains. Initial analytic analysis of convection in a rotating sphere (Chandrasekhar, 1961; Roberts, 1968; Busse, 1970), were extended to to numerical linear and nonlinear numerical studies aimed at understanding the behavior of rotating turbulent astrophysical bodies (Gilman, 1975, 1977). In particular, the aim was to understand the importance of nonlinear process in both the solar (Gilman, 1979) and terrestrial (Cuong and Busse, 1981) contexts. In the solar case, this was strongly motivated by the need to explain solar differential rotation, which had at the time been observed for more than one century (Carrington, 1860).

The earliest numerical calculations were done using the Boussinesq approximation, but quickly extended to include stratification using the anelastic approximation, as discussed in the previous section (Gilman and Glatzmaier, 1981; Glatzmaier and Gilman, 1982). At the same time, dynamo calculations were solving for the evolution of a magnetic field in these simulations, adding new theoretical constraints on the understanding of its generation within the Sun (Gilman and Miller, 1981; Glatzmaier, 1984, 1985). In parallel, stellar evolution models became sophisticated enough to model in detail the solar stratification (i.e., density, pressure, temperature, equation-of-state, opacity as functions of depth) and these models were found to be highly consistent with deductions based on helioseismic measurements (Model S: Christensen-Dalsgaard et al, 1996). With the stratification well modeled, notable advances could be made in a more realistic reproduction of thermal convection (e.g., Miesch et al, 2000; Brun and Toomre, 2002). Although spatial resolutions were moderate ($N_\theta < 128$, $\ell_{\max} < 85$), the differential rotation profile of the Sun, with a fast equator, was reproduced in these anelastic studies.

However, the differential-rotation profiles with depth differed. The differential-rotation profiles found in numerical solutions tended to obey the Taylor-Proudman theorem, i.e., $\partial\langle\Omega\rangle/\partial z = 0$. Measurements of the rotation rate inside the Sun show that the dynamics there does not. Motivated by a thorough assessment of mean-field dynamics (Rempel, 2005), Miesch et al (2006) adopted latitudinal entropy gradient at the bottom boundary and achieved non-Taylor-Proudman differential rotation, as indeed is suggested by Equation 16 above. This somewhat ad-hoc method was adopted by several follow-up studies (e.g. Miesch et al, 2008; Fan and Fang, 2014), with a more self-consistent approach by Brun et al (2011), which includes aspects of overshoot layer between the convection zone and the deeper radiative layer below, suggesting that the interaction between the two layers is responsible for the crucial latitudinal entropy gradient, the tachocline, and the conical profile observed in the bulk of the convection zone.

This conclusion has not gone without debate. Earlier, Miesch et al (2000) concluded that anisotropic entropy transport by the overshooting downflows may not be enough to maintain a solar-like differential rotation profile, though

Hotta (2018) point out that an efficient small-scale dynamo can amplify the effect (see also Hotta et al, 2015a), and help produce required non-Taylor-Proudman state. Recently Matilsky et al (2020) have pointed out that the latitudinal entropy gradient achieved is sensitive to the radial boundary condition imposed. Resolution of these uncertainties is critical to our understanding of the origin of the observed radial profile of the solar differential rotation.

The other non-Taylor-Proudman feature in the solar convection zone is the near-surface shear layer (NSSL). Since the NSSL is located in the near-surface where the Rossby number is high, i.e., the rotational influence is weak, its origin is thought to lie with advection, $\nabla \times (\boldsymbol{v} \times \boldsymbol{\omega})$ in the vorticity equation. Numerical simulations have succeeded in reproducing part of the observed feature (Guerrero et al, 2013; Hotta et al, 2015b; Matilsky et al, 2019), with turbulent viscosity playing an important role Hotta et al (2015b), however, the models fail to reproduce key aspects of the NSSL, especially at mid-latitude. Matilsky et al (2019) argue that the role of large scale columnar convection (banana cells) and meridional circulation and their balance differ with latitude, but are unable to produce a solution that captures the NSSL in both the equatorial and high-latitude regions. Overall, a consensus has not been reached on the maintenance mechanism for the NSSL.

The gaps in our understanding of large scale-flows in the Sun all reflect a more fundamental difficulty that has come to be known as the *convective conundrum*. The amplitudes of the motions in simulations of solar convection are significantly higher at low wavenumbers than most solar observations suggest. This means that they are more weakly rotationally constrained, with consequent implications for global scale flows. This will be addressed in more detail in Section 3.

## 2.6 Toward modeling of other stars

Using models such as the ones presented previously, numerical simulations are a powerful tool to study the formation and dynamics of large-scale flows in the astrophysical context. In particular, full sphere simulations, resolving a broad range of turbulent convective scales, are suitable tools to probe the solar interior as well as constrain the large-scale dynamics of distant stars. As examples, numerical studies of solar-type stars recently provided new constraints on the trends we can expect for differential rotation ($\Delta\Omega \propto \Omega_*^{0.46}$) on G and K stars (Brun et al, 2022), and highlight the different large-scale flows regimes possible. These regimes can be characterized by the dimensionless Rossby number, which quantifies the rotational constraint of the Coriolis force on convective motions (Gastine et al, 2014; Brun and Browning, 2017; Hindman et al, 2020).

Thanks to numerical simulations (Matt et al, 2011; Guerrero et al, 2013; Käpylä et al, 2014; Simitev et al, 2015; Brun et al, 2017; Karak et al, 2018), three regimes are currently acknowledged in global rotating models of main-sequence solar-type stars: 1. At low Rossby numbers, differential rotation profiles are highly constrained (Taylor-Proudman) with flows that become cylindrical (Gilman, 1975; Elliott et al, 2000; Miesch et al, 2006; Brown et al,

2008). In extreme cases, such profiles show alternating prograde and retrograde zonal jets, also called Jupiter-like jets (Rhines, 1975; Heimpel et al, 2016). The meridional circulations under these conditions is typically multicellular in each hemisphere and aligned along the vertical axis (see for example Brun et al 2017). When magnetic fields are included in the calculation, the Lorentz force feedback can quench the flows, (Brun, 2004; Yadav et al, 2015), resulting in a significant decrease of the differential rotation contrast ($\Omega$-quenching) and the appearance of trans-equatorial meridional-circulation cells (Brun et al, 2022). 2. At intermediate Rossby numbers, the differential rotation adopts a typical solar-like conical profile, with a fast equator and slow poles (Figure 1, see for instance Miesch et al 2006; Hotta et al 2022). In this regime the power sustaining the differential rotation contrast can reach tens of percent of the stellar luminosity (Brun et al, 2022). 3. At high Rossby number (typically over the unity), differential-rotation profiles in simulations become "anti-solar" (Gastine et al, 2014), showing then a slow equator and fast poles (Gilman, 1977). Unlike the previous regime, this has so far not been clearly detected on main-sequence stars. An active search is currently underway to better constrain this regime for solar-type stars (Reiners, 2007; Reinhold and Arlt, 2015; Benomar et al, 2018; Noraz et al, 2022a).

As stars spin down along the main sequence (Skumanich, 1972; Gallet and Bouvier, 2013; Ahuir et al, 2021), the Rossby number is expected to increase, and transitions between these large-scale flow regimes may influence the evolution of the star (Metcalfe et al, 2022). In particular, large scale flows play important roles in global dynamo processes and the magnetic fields produced by a star could change in nature (Karak et al, 2015; Warnecke, 2018; Viviani et al, 2019; Brun et al, 2022; Noraz et al, 2022b). Large-scale flows and magnetism are strongly entwined and impacted by the influence of the evolution of rotational influences on the turbulent convection.

Recent observations show that the composition of the star too plays a role in the convective dynamo (See et al, 2021). One-dimensional stellar models show varying sensitivities to metallicity (Amard and Matt (2020), see also Section 4 of Noraz et al (2022a) for a discussion). Typically, when metallicity is increased at a given stellar mass and age, the opacity also increases, and thus so too does the temperature gradient within the star. The convective zone becomes deeper in proportion to the stellar radius, with longer convective turnover times at its base because of the higher inertia induced by a higher density. This then likely modifies the convective scale distribution and also decrease the Rossby number of the star, which subsequently impacts the dynamics of the large-scale flows (Bessolaz and Brun, 2011). Such metallicity effects may lie at the origin of the observed differences in the magnetism of HD 173701 (mentioned in Section 1.4). Karoff et al (2018) suggest that the higher metallicity of that star could either enhance the magnetic field generated or the observed facular contrast, yielding then the large amplitude brightness variations observed during the activity cycle. Comparisons between solar twins of different metallicities are needed to either confirm or decipher such mechanisms. To guide

those observations, local-area numerical studies of the metalicity impact on photospheric convection have already started (Witzke et al, 2022), and studies using global simulations are currently being investigated (Noraz, 2022).

# 3 Discrepancies between observations and models and possible solutions

Significant difficulties remain when making direct comparison of the observed large scale motions on the Sun and those produced in numerical simulations still exist. Most fundamentally, until recently (Hotta and Kusano, 2021), all global spherical shell models of global convection and circulation produced anti-solar differential rotation profiles (a slow equator and a fast pole) at solar rotation rates, and no local area models of solar convection produces a peak in the photospheric horizontal velocity a supergranular scales, as observed. These discrepancies likely reflect a mismatch in convective amplitudes at depth, that has been come to be known as the 'convective conundrum' (O'Mara et al, 2016). The global implications were first recognized when increased numerical resolution in simulations resulted in lower diffusivity, faster convective flows, and consequent difficulty in achieving a solar-like differential rotation profile (Miesch et al, 2008).

## 3.1 The convection conundrum

There is an observation mismatch between flow velocities on the Sun and those found in numerical simulations. In the surface layers this is dramatically illustrated by the ubiquitous and dominating presence of giant cells in global numerical simulations, the difficulty of identifying them in observations, and the absence of supergranulation in local area models, compared to its importance in photospheric observations. That aspect of the convective conundrum is discussed in Section 1.2 and 2.2 above. In summary, these disparities suggest reduced convective amplitudes with depth, by a factor of about 2.5 below 10 Mm, with several causes for this reduction suggested in the literature, any one or more of which would suffice.

Convective amplitudes in the near solar surface region of the solar convection zone can be measured using a variety of local helioseismic techniques. As illustrated by Figure 5 these do not agree with each other or with numerical simulations (Hanasoge et al, 2012; Gizon and Birch, 2012; Greer et al, 2015). In general models produce flow with significant power at low wavenumbers, monotonically increasing to low wavenumber, while observations indicate reduced power there. A modeling exception is the recent Hotta and Kusano (2021) simulation, in which the horizontal velocity power rolls over at large scales, though at scales somewhat beyond that of supergranulation. An observational exception is the ring-diagram result of Greer et al (2015) which shows significant power at scales larger than supergranulation at a depth of 0.96 $R_\odot$.

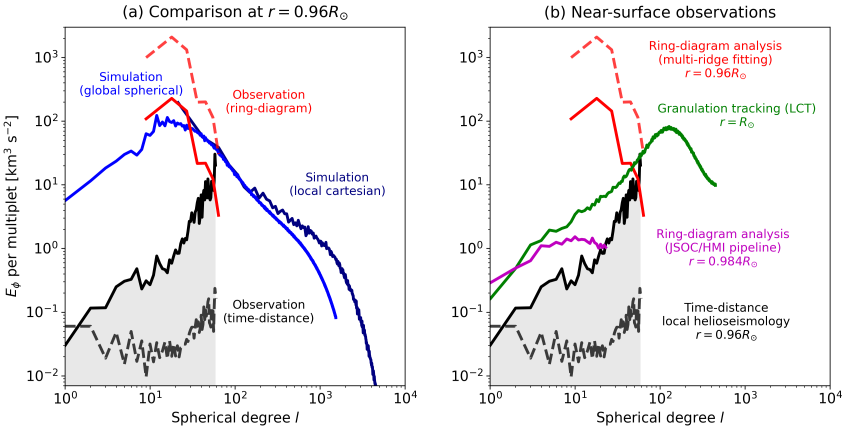


**Fig. 5** Horizontal velocity power spectra near the solar surface. (a) Comparison of the spectra between numerical simulations and the observations at $r = 0.96R_\odot$ (Birch, 2023). *Blue*: A global full-spherical simulation of rotating magneto-convection by Hotta and Kusano (2021). *Navy*: A local cartesian box simulation of solar convection by Hotta et al (2019). *Black*: An upper limit infered by deep-focusing time-distance helioseismic measurements. Dashed and solid lines show the original results of Hanasoge et al (2012) and the revised results (Proxauf, 2020). (b) Comparison of the spectra obtained by various observational measurements at various depths. *Red*: Multi-ridge fitting ring-diagram analysis by Greer et al (2015). Dashed and solid lines show their original results and the revised results (Nagashima et al, 2020). *Green*: Local correlation tracking of surface granulation (Proxauf, 2020). *Magenta*: The SDO/HMI ring-diagram pipeline (Bogart et al, 2011a,b; Proxauf, 2020). All observations reported ion the above plots are available online (Birch, 2023).

While refinement and revisions of the techniques employed have brought measurements and models closer together, there are significant and important remaining discrepancies. It is imperative to resolve these, not just to understand the Sun and its dynamo, but because the solar case serves as the touchstone for stellar modeling.

## 3.2 Columnar convective modes

Mixing-length models suggest that the typical scale of convection is determined by the background density scale height (e.g., Lord et al, 2014). A hierarchy of convective scales is therefore expected in the Sun, from granulation at $1-2$ Mm, supergranulation at $20-30$ Mm, and to giant-cell convection at $100-200$ Mm (Rieutord and Rincon, 2010, see also Section 1.2 above and references therein). Numerical simulations of rotating convection have repeatedly found that the giant-cell convection tends to exist as *banana cells* in a strongly rotationally-constrained regime (e.g., Miesch et al, 2000). These banana cells are located outside the tangential cylinder and can be seen as north-south aligned downflow lanes across the equator. They are known to propagate in a prograde direction with frequencies higher than the local differential rotation rate (Miesch et al, 2008).

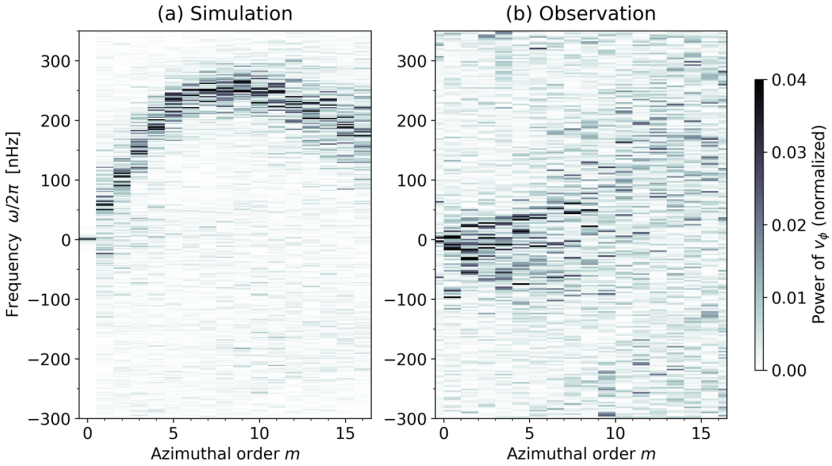


**Fig. 6** Sectoral component of longitudinal velocity power spectra near the surface. The power is normalized at each azimuthal order $m$. All the frequencies are computed in a Carrington frame ($\Omega_{\rm car}/2\pi = 456.0$ nHz). (a) Simulated power spectra from a solar-like rotating convection simulation (Bekki et al, 2022a). (b) Observational power spectra obtained by the ring-diagram analysis with 15° tile size (Proxauf et al, 2020).

The prograde propagation of banana cells can be understood in terms of a special class of inertial modes called *columnar convective modes* or *thermal Rossby modes* (e.g., Busse, 2002; Miesch et al, 2008; Bekki et al, 2022a). They are $z$-vorticity waves arising from the compressional $\beta$-effect due to the strong background density stratification. A linear dispersion relation of the columnar convective modes was first derived by Glatzmaier and Gilman (1981) using a cylindrical model and later by Hindman and Jain (2022) in Cartesian geometry. The most realistic spherical-shell model has recently been presented by Bekki et al (2022b). They have shown that the dispersion relation of the columnar convective modes is very sensitive to the superadiabaticity $\delta$, and that the modes become convectively-unstable (exponentially growing) when the background is slightly superadiabatic ($\delta > 0$). These modes have the associated Reynolds stress $\langle v_r v_\phi \rangle > 0$ and $\langle v_\theta v_\phi \rangle > 0$ in the northern hemisphere ($\langle v_\theta v_\phi \rangle < 0$ in the southern hemisphere), implying that they transport the angular momentum radially upward and equatorward outside the tangential cylinder. The great importance of *banana cells* on the establishment of the solar-like differential rotation has been repeatedly appreciated in previous literature (Käpylä et al, 2011; Gastine et al, 2013; Hotta et al, 2015b; Matilsky et al, 2020; Camisassa and Featherstone, 2022).

Despite their significant importance, as shown in Fig. 6 columnar convective modes have never been observed on the surface of the Sun, though very large-scale flows have been deduced from correlation tracking of the solar supergranulation (Hathaway et al, 2013; Hathaway and Upton, 2021) and possible indirect evidence for these flows comes from measured alignment of the solar supergranulation (Lisle et al, 2004; Nagashima et al, 2011). It remains a

mystery why the columnar convective modes are not directly detected in the solar surface observations. One possible scenario is that they indeed exist hidden in the deep convection zone with substantial amplitudes but are concealed by surface small-scale convective feature (Guerrero et al, 2013). The other scenario is that they are simply absent in the Sun (or too weak to be detected (van Ballegooijen, 1986; Lord et al, 2014, Section 2.2 above). If the latter is the case, the angular momentum needs to be transport by something other than the Reynolds stress. Recent high-resolution simulations suggest that the small-scale Maxwell stress can transport the angular momentum equatorward to accelerate the equator (Hotta et al, 2022). If this so-called *punching-ball* effect prevails in the Sun, the columnar convective modes might no longer be required to establish the solar differential rotation.

## 3.3 Differential rotation

An important aspect of the convective conundrum is its implications for differential rotation. In early phase of the solar differential rotation research, the solar differential rotation profile could be reproduced relatively easily. As supercomputer power grew, allowing simulation of higher resolution, the problem became apparent. Simulations began to fail to reproduce the solar-like differential rotation profile at solar rotation rates.

A well-known feature of differential rotation is that a fast equator (poles) is obtained with strong (weak) rotational influence (e.g., Gastine et al, 2013; Featherstone and Miesch, 2015; Karak et al, 2015). The rotational influence is measured by the Rossby number $\mathrm{Ro} = v/(2\Omega L)$, where $v$, and $L$ are the typical convection velocity and spatial scales respectively. Although we believed that the Sun is in a low Rossby-number regime, high resolution simulations most often produce anti-solar differential rotation profiles (fast poles). High resolution simulations introduce the small-scale turbulence which is important for heat transport but is only very weakly rotationally constrained. This has been recently confirmed with scale-dependence analyses of the angular momentum flux (Mori and Hotta, 2023). The small-scale turbulence tends to transport the angular momentum radially inward which leads one-cell meridional flow, which transports angular momentum and accelerate the poles (see also Featherstone and Miesch, 2015). In other words, high-resolution decreases the typical convection scale $L$ placing the simulation in a high Rossby number regime, resulting an anti-solar differential rotation.

Three mechanisms have been employed in global simulations in order to maintain a solar-like differential rotation profile, i.e, to maintain the low Rossby number, in the face of vigorous smaller-scale convective flows.

- Increasing the rotation rate $\Omega_0$ (Brown et al, 2008; Nelson et al, 2013; Hotta, 2018).
- Reducing the luminosity $L_\odot$ (Hotta et al, 2015b), which leads to reduction of $v$.

- Increasing viscosity $\nu$ and/or thermal conductivity $\kappa$ (Miesch et al, 2000, 2008; Fan and Fang, 2014; Hotta et al, 2016), which leads to reduction of $v$ and increase of $L$.

None of these reflect a possible physical mechanism operating on the Sun but not captured in simulations. They cannot provide an answer to the question: Why does the Sun have such a low Rossby number?

Recently, Hotta and Kusano (2021) reproduced the solar-like differential rotation in extremely high resolution simulation without using these manipulations. Hotta et al (2022) showed that in that simulation the strong magnetic field maintained by the convection when the magnetic diffusivity is very low, as it is in their simulation, causes angular momentum to be transported outward. Double-cell meridional flow is generated and that flow transports angular momentum equatorward, resulting in the solar-like differential rotation profile achieved. An important point is that the Hotta and Kusano (2021) simulation convection remains in a high Rossby number regime but the banana-cells no longer play an dominant role in the angular momentum transport.

# 4 Future prospects

From a theoretical view point, some more significant progress can be made in the near future. Hotta and Kusano (2021) show that the high-resolution simulations remain a promising approach to understand the solar large-scale flows. Simulations have not yet reached *numerical convergence*, where by numerical convergence we mean that when we double the resolution the large-scale structure does not change. The solar convective turbulence in the simulations has too broad a spectral, with more power at low wavenumbers than likely the case for the Sun. With the injection scale at 200 Mm and the dissipation scale is around 1 cm, it will remain very difficult to directly resolve all the energy containing scales with numerical simulations. It may only be possible to reach the numerical convergence only when all the scales are captured. In that case, we need to construct reliable turbulence models which can mimic the essential features of unresolved flows.

Such models require a deep understanding of the key physical components of the convection. Important progress has been made in understanding the essential role of rotation (e.g., Vasil et al, 2021, and references therin) and preliminary work has begun to characterize the highly nonlocal convective flows that result from radiative cooling of the photosphere which may play an important role in heat transport heat and allow a mean gradient much closer to isentropic than that achieved by current simulations (Brandenburg, 2016; Cossette and Rast, 2016). Moreover, radiative heating of the lower convection zone likely plays an important role, one that has only begun to be examined. Brun et al (2011) have undertook an important study of the interaction between the convection and radiation zone, but, as Käpylä (2019) pointed out, a fully consistent treatment of the overshoot layer requires huge numerical resources,

which are currently not available (see also Hotta, 2017). Solving these convective aspects of the convective conundrum is essential to understanding the large-scale flow dynamics.

Another direct approach is to combine in one simulation the radiative magnetohydrodynamics of the photosphere and the global scale convective motions. Including the photosphere may have a significant impact on the deep large-scale convection (Spruit, 1997). Hotta et al (2019) found only weak (or no) influence from the photosphere on the deep convection, however their result may not reflect a lack of importance of these flows, but the difficulties faced in maintaining them with depth given the diffusivities required in global models. Even when the resolution of the simulation is increased (and numerical or explicit diffusivities are reduced), the problem persists because the horizontal scales of the flow structures are also decreases. What is required to maintain nonlocal transport in a simulation is that the diffusion time across a downflowing plume be greater than the transit time of that fluid across the fluid layer. This is extremely difficult to achieve. Because of the steep stratification, local area radiative magnetohydrodynamic simulations, and ambitious global models which include an upper radiative boundary, may be able to produce granular scale downflow structures but not the low thermal diffusivity required for them to maintain their role in transport at depth.

Over the past fifty years, tremendous progress has been made in understanding and simulating solar convection and the global scale flows that result in a rotating domain. The Sun allows us to directly confront that progress with observations, observations that, with the advent and development of helioseismology over the same time period, have also made previously unimaginable advances. New diagnostics based on the study of the solar inertial modes are expected to provide additional constraints on the physics of the convection zone. Some gaps in the observations and some fundamental issues in our understanding however remain. Resolving those will not only advance our understanding of the origin of large-scale global flows, but will also allow us to more robustly model the solar dynamo, perhaps predict solar behavior critical to human activities in space and on Earth, and extend our understanding to other stars for which comparison with data will remain less constraining. Understanding the Sun is thus a touchstone activity.

**Acknowledgments.** We acknowledge the support from ISSI Bern for our participation in the workshop. We thank Zhi-Chao Liang for helpful comments on the manuscript. HH is supported by JSPS KAKENHI grant Nos. JP20K14510, JP21H04492, JP21H01124, JP21H04497, and MEXT as a Program for Promoting Researches on the Supercomputer Fugaku ("Toward a unified view of the universe: from large-scale structures to planets," grant No. 20351188). YB, LG and QN acknowledge financial support from ERC Synergy Grant WHOLE SUN 810218. QN was funded in part by an INSU/PNST grant and CNES (Solar Orbiter). MPR acknowledges partial support for this work by the National Science Foundation under award number NSF 1841100.

## Ethics Declarations

**Competing interests** The authors declare they have no conflicts of interest.

## References

Ahuir J, Strugarek A, Brun AS, et al (2021) Magnetic and tidal migration of close-in planets: Influence of secular evolution on their population. Astronomy & Astrophysics 650:A126. https://doi.org/10.1051/0004-6361/202040173

Amard L, Matt SP (2020) The Impact of Metallicity on the Evolution of the Rotation and Magnetic Activity of Sun-like Stars. The Astrophysical Journal 889(2):108. https://doi.org/10.3847/1538-4357/ab6173

Balona LA, Abedigamba OP (2016) Differential rotation in K, G, F and A stars. Monthly Notices of the Royal Astronomical Society 461(1):497–506. https://doi.org/10.1093/mnras/stw1443

Barnes JR, Cameron AC, Donati JF, et al (2005) The dependence of differential rotation on temperature and rotation. Monthly Notices of the Royal Astronomical Society: Letters 357(1):L1–L5. https://doi.org/10.1111/j.1745-3933.2005.08587.x

Basu S, Antia HM (2010) Characteristics of Solar Meridional Flows during Solar Cycle 23. ApJ717(1):488–495. https://doi.org/10.1088/0004-637X/717/1/488, https://arxiv.org/abs/arXiv:1005.3031 [astro-ph.SR]

Bazot M, Benomar O, Christensen-Dalsgaard J, et al (2019) Latitudinal differential rotation in the solar analogues 16 Cygni A and B. Astronomy & Astrophysics 623:A125. https://doi.org/10.1051/0004-6361/201834594

Beck PG, Montalban J, Kallinger T, et al (2012) Fast core rotation in red-giant stars as revealed by gravity-dominated mixed modes. Nature481(7379):55–57. https://doi.org/10.1038/nature10612, https://arxiv.org/abs/arXiv:1112.2825 [astro-ph.SR]

Bekki Y, Cameron RH (2023) Three-dimensional non-kinematic simulation of the post-emergence evolution of bipolar magnetic regions and the Babcock-Leighton dynamo of the Sun. A&A670:A101. https://doi.org/10.1051/0004-6361/202244990, https://arxiv.org/abs/arXiv:2209.08178 [astro-ph.SR]

Bekki Y, Hotta H, Yokoyama T (2017) Convective Velocity Suppression via the Enhancement of the Subadiabatic Layer: Role of the Effective Prandtl Number. ApJ851(2):74. https://doi.org/10.3847/1538-4357/

aa9b7f, https://arxiv.org/abs/arXiv:1711.05960 [astro-ph.SR]

Bekki Y, Cameron RH, Gizon L (2022a) Theory of solar oscillations in the inertial frequency range: Amplitudes of equatorial modes from a non-linear rotating convection simulation. A&A666:A135. https://doi.org/10.1051/0004-6361/202244150, https://arxiv.org/abs/arXiv:2208.11081 [astro-ph.SR]

Bekki Y, Cameron RH, Gizon L (2022b) Theory of solar oscillations in the inertial frequency range: Linear modes of the convection zone. A&A662:A16. https://doi.org/10.1051/0004-6361/202243164, https://arxiv.org/abs/arXiv:2203.04442 [astro-ph.SR]

Benomar O, Bazot M, Nielsen MB, et al (2018) Asteroseismic detection of latitudinal differential rotation in 13 Sun-like stars. Science 361(6408):1231–1234. https://doi.org/10.1126/science.aao6571

Berrilli F, Del Moro D, Russo S, et al (2005) Spatial Clustering of Photospheric Structures. ApJ632(1):677–683. https://doi.org/10.1086/432708

Berrilli F, Scardigli S, Giordano S (2013) Multiscale Magnetic Underdense Regions on the Solar Surface: Granular and Mesogranular Scales. Sol. Phys.282(2):379–387. https://doi.org/10.1007/s11207-012-0179-2, https://arxiv.org/abs/arXiv:1208.2669 [astro-ph.SR]

Bessolaz N, Brun AS (2011) Hunting for giant cells in deep stellar convective zones using wavelet analysis. The Astrophysical Journal 728(2):115. https://doi.org/10.1088/0004-637X/728/2/115

Bhattacharya J, Hanasoge SM (2022) A spectral solver for solar inertial waves. arXiv e-prints arXiv:2211.03323. https://arxiv.org/abs/arXiv:2211.03323 [astro-ph.SR]

Birch A (2023) Convection Spectra from the Thesis of B. Proxauf. https://doi.org/10.17617/3.DFU3SQ, URL https://doi.org/10.17617/3.DFU3SQ

Bogart RS, Baldner C, Basu S, et al (2011a) HMI ring diagram analysis I. The processing pipeline. In: GONG-SoHO 24: A New Era of Seismology of the Sun and Solar-Like Stars, p 012008, https://doi.org/10.1088/1742-6596/271/1/012008

Bogart RS, Baldner C, Basu S, et al (2011b) HMI ring diagram analysis II. Data products. In: GONG-SoHO 24: A New Era of Seismology of the Sun and Solar-Like Stars, p 012009, https://doi.org/10.1088/1742-6596/271/1/012009

Böhm-Vitense E (1958) Über die Wasserstoffkonvektionszone in Sternen verschiedener Effektivtemperaturen und Leuchtkräfte. Mit 5 Textabbildungen. Zeitschrift für Astrophysik 46:108

Böning VGA, Roth M, Jackiewicz J, et al (2017) Inversions for Deep Solar Meridional Flow Using Spherical Born Kernels. ApJ845(1):2. https://doi.org/10.3847/1538-4357/aa7af0, https://arxiv.org/abs/arXiv:1707.08803 [astro-ph.SR]

Braginsky SI, Roberts PH (1995) Equations governing convection in earth's core and the geodynamo. Geophysical & Astrophysical Fluid Dynamics 79(1-4):1–97. https://doi.org/10.1080/03091929508228992

Brandenburg A (2016) Stellar Mixing Length Theory with Entropy Rain. ApJ832(1):6. https://doi.org/10.3847/0004-637X/832/1/6, https://arxiv.org/abs/arXiv:1504.03189 [astro-ph.SR]

Braun DC, Fan Y (1998) Helioseismic Measurements of the Subsurface Meridional Flow. ApJL 508:L105–L108. https://doi.org/10.1086/311727

Braun DC, Birch AC, Fan Y (2021) Probing the Solar Meridional Circulation Using Fourier Legendre Decomposition. ApJ911(1):54. https://doi.org/10.3847/1538-4357/abe7e4, https://arxiv.org/abs/arXiv:2103.02499 [astro-ph.SR]

Brown BP, Browning MK, Brun AS, et al (2008) Rapidly Rotating Suns and Active Nests of Convection. The Astrophysical Journal 689(2):1354–1372. https://doi.org/10.1086/592397

Brown BP, Vasil GM, Zweibel EG (2012) Energy conservation and gravity waves in sound-proof treatments of stellar interiors. Part I. Anelastic approximations. The Astrophysical Journal 756(2):109. https://doi.org/10.1088/0004-637X/756/2/109

Brun AS (2004) On the interaction between differential rotation and magnetic fields in the Sun. Solar Physics 220(2):333–344. https://doi.org/10.1023/B:SOLA.0000031384.75850.68

Brun AS, Browning MK (2017) Magnetism, dynamo action and the solar-stellar connection. Living Reviews in Solar Physics 14(1). https://doi.org/10.1007/s41116-017-0007-8

Brun AS, Toomre J (2002) Turbulent Convection under the Influence of Rotation: Sustaining a Strong Differential Rotation. The Astrophysical Journal 570(2):865–885. https://doi.org/10.1086/339228

Brun AS, Miesch MS, Toomre J (2011) Modeling the Dynamical Coupling of Solar Convection with the Radiative Interior. ApJ742(2):79. https://doi.org/10.1088/0004-637X/742/2/79

Brun AS, Strugarek A, Varela J, et al (2017) On Differential Rotation and Overshooting in Solar-like Stars. The Astrophysical Journal 836(2):192. https://doi.org/10.3847/1538-4357/aa5c40

Brun AS, Strugarek A, Noraz Q, et al (2022) Powering Stellar Magnetism: Energy Transfers in Cyclic Dynamos of Sun-like Stars. The Astrophysical Journal 926(1):21. https://doi.org/10.3847/1538-4357/ac469b

Busse FH (1970) Thermal instabilities in rapidly rotating systems. Journal of Fluid Mechanics 44(3):441–460. https://doi.org/10.1017/S0022112070001921

Busse FH (2002) Convective flows in rapidly rotating spheres and their dynamo action. Phys Fluids 14(4):1301–1314. https://doi.org/10.1063/1.1455626

Camisassa ME, Featherstone NA (2022) Solar-like to Antisolar Differential Rotation: A Geometric Interpretation. ApJ938(1):65. https://doi.org/10.3847/1538-4357/ac879f, https://arxiv.org/abs/arXiv:2208.05591 [astro-ph.SR]

Canfield RC, Mehltretter JP (1973) Fluctuations of Brightness and Vertical Velocity at Various Heights in the Photosphere. Sol. Phys.33(1):33–48. https://doi.org/10.1007/BF00152375

Carrington RC (1860) On two cases of Solar Spots in High Latitudes, and on the Surface Currents indicated by the Observations. MNRAS20:254. https://doi.org/10.1093/mnras/20.6.254

Cattaneo F, Lenz D, Weiss N (2001) On the Origin of the Solar Mesogranulation. ApJ563(1):L91–L94. https://doi.org/10.1086/338355

Chandrasekhar S (1961) Hydrodynamic and hydromagnetic stability. Dover Publications, Inc. New York

Charbonneau P (2020) Dynamo models of the solar cycle. Living Reviews in Solar Physics 17(1):4. https://doi.org/10.1007/s41116-020-00025-6

Chen R, Zhao J (2017) A Comprehensive Method to Measure Solar Meridional Circulation and the Center-to-limb Effect Using Time-Distance Helioseismology. ApJ849(2):144. https://doi.org/10.3847/1538-4357/aa8eec, https://arxiv.org/abs/arXiv:1709.07905 [astro-ph.SR]

Christensen-Dalsgaard J, Däppen W, Ajukov SV, et al (1996) The Current State of Solar Modeling. Science 272(5266):1286–1292. https://doi.org/10.1126/science.272.5266.1286

Clune T, Elliott J, Miesch M, et al (1999) Computational aspects of a code to study rotating turbulent convection in spherical shells. Parallel Computing 25(4):361–380. https://doi.org/10.1016/S0167-8191(99)00009-5

Collier Cameron A (2007) Differential rotation on rapidly rotating stars. Astronomische Nachrichten 328(10):1030–1033. https://doi.org/10.1002/asna.200710880

Cossette JF, Rast MP (2016) Supergranulation as the Largest Buoyantly Driven Convective Scale of the Sun. ApJ829(1):L17. https://doi.org/10.3847/2041-8205/829/1/L17, https://arxiv.org/abs/arXiv:1606.04041 [astro-ph.SR]

Cranmer SR, Saar SH (2011) Testing a predictive theoretical model for the mass loss rates of cool stars. The Astrophysical Journal 741(1):54. https://doi.org/10.1088/0004-637X/741/1/54

Crouch AD, Charbonneau P, Thibault K (2007) Supergranulation as an Emergent Length Scale. ApJ662(1):715–729. https://doi.org/10.1086/515564

Cuong P, Busse F (1981) Generation of magnetic fields by convection in a rotating sphere, I. Physics of the Earth and Planetary Interiors 24(4):272–283. https://doi.org/10.1016/0031-9201(81)90114-X

Deheuvels S, García RA, Chaplin WJ, et al (2012) Seismic evidence for a rapidly rotating core in a lower-giant-branch star observed with *KEPLER*. The Astrophysical Journal 756(1):19. https://doi.org/10.1088/0004-637X/756/1/19

Deheuvels S, Ballot J, Eggenberger P, et al (2020) Seismic evidence for near solid-body rotation in two *Kepler* subgiants and implications for angular momentum transport. Astronomy & Astrophysics 641:A117. https://doi.org/10.1051/0004-6361/202038578

Demarque PR, Percy JR (1964) A Series of Solar Models. ApJ140:541. https://doi.org/10.1086/147947

Donahue RA, Saar SH, Baliunas SL (1996) A Relationship between Mean Rotation Period in Lower Main-Sequence Stars and Its Observed Range. ApJ466:384. https://doi.org/10.1086/177517

Duvall JT. L. (1979) Large-scale solar velocity fields. Sol. Phys.63(1):3–15. https://doi.org/10.1007/BF00155690

Duvall JT. L., Birch AC (2010) The Vertical Component of the Supergranular Motion. ApJ725(1):L47–L51. https://doi.org/10.1088/2041-8205/725/1/L47

Duvall JT. L., Hanasoge SM (2009) Measuring Meridional Circulation in the Sun. In: Dikpati M, Arentoft T, González Hernández I, et al (eds) Solar-Stellar Dynamos as Revealed by Helio- and Asteroseismology: GONG 2008/SOHO 21, p 103, 0905.3132

Duvall JT. L., Dziembowski WA, Goode PR, et al (1984) Internal rotation of the Sun. Nature310(5972):22–25. https://doi.org/10.1038/310022a0

Duvall TLJr., Jefferies SM, Harvey JW, et al (1993) Time-distance helioseismology. Nature 362:430–432. https://doi.org/10.1038/362430a0

Elliott JR, Miesch MS, Toomre J (2000) Turbulent Solar Convection and Its Coupling with Rotation: The Effect of Prandtl Number and Thermal Boundary Conditions on the Resulting Differential Rotation. ApJ533(1):546–556. https://doi.org/10.1086/308643

Falco M, Puglisi G, Guglielmino SL, et al (2017) Comparison of different populations of granular features in the solar photosphere. A&A605:A87. https://doi.org/10.1051/0004-6361/201629881

Fan Y, Fang F (2014) A Simulation of Convective Dynamo in the Solar Convective Envelope: Maintenance of the Solar-like Differential Rotation and Emerging Flux. ApJ789(1):35. https://doi.org/10.1088/0004-637X/789/1/35, https://arxiv.org/abs/arXiv:1405.3926 [astro-ph.SR]

Featherstone NA, Hindman BW (2016) The Emergence of Solar Supergranulation as a Natural Consequence of Rotationally Constrained Interior Convection. ApJ830(1):L15. https://doi.org/10.3847/2041-8205/830/1/L15, https://arxiv.org/abs/arXiv:1609.05153 [astro-ph.SR]

Featherstone NA, Miesch MS (2015) Meridional Circulation in Solar and Stellar Convection Zones. ApJ804(1):67. https://doi.org/10.1088/0004-637X/804/1/67, https://arxiv.org/abs/arXiv:1501.06501 [astro-ph.SR]

Gallet F, Bouvier J (2013) Improved angular momentum evolution model for solar-like stars. Astronomy & Astrophysics 556:A36. https://doi.org/10.1051/0004-6361/201321302

García RA, Ballot J (2019) Asteroseismology of solar-type stars. Living Reviews in Solar Physics 16(1):4. https://doi.org/10.1007/s41116-019-0020-1

Gastine T, Wicht J, Aurnou JM (2013) Zonal flow regimes in rotating anelastic spherical shells: An application to giant planets. Icarus225(1):156–172. https://doi.org/10.1016/j.icarus.2013.02.031, https://arxiv.org/abs/arXiv:1211.3246 [astro-ph.EP]

Gastine T, Yadav RK, Morin J, et al (2014) From solar-like to antisolar differential rotation in cool stars. Monthly Notices of the Royal Astronomical Society: Letters 438(1):L76–L80. https://doi.org/10.1093/mnrasl/slt162

Giles PM (2000) Time-distance measurements of large-scale flows in the solar convection zone. PhD thesis, Stanford University, California

Giles PM, Duvall TL, Scherrer PH, et al (1997) A subsurface flow of material from the Sun's equator to its poles. Nature 390:52–54. https://doi.org/10.1038/36294

Gilman PA (1975) Linear Simulations of Boussinesq Convection in a Deep Rotating Spherical Shell. Journal of Atmospheric Sciences 32(7):1331–1352

Gilman PA (1977) Nonlinear Dynamics of Boussinesq Convection in a Deep Rotating Spherical Shell. I. Geophysical and Astrophysical Fluid Dynamics 8:93–135. https://doi.org/10.1080/03091927708240373

Gilman PA (1979) Model calculations concerning rotation at high solar latitudes and the depth of the solar convection zone. The Astrophysical Journal 231:284. https://doi.org/10.1086/157191

Gilman PA, Glatzmaier GA (1981) Compressible convection in a rotating spherical shell. I. Anelastic equations. The Astrophysical Journal Supplement Series 45(2):53

Gilman PA, Miller J (1981) Dynamically consistent nonlinear dynamos driven by convection in a rotating spherical shell. The Astrophysical Journal Supplement Series 46:211. https://doi.org/10.1086/190743

Gizon L (2004) Helioseismology of Time-Varying Flows Through The Solar Cycle. Sol. Phys.224(1-2):217–228. https://doi.org/10.1007/s11207-005-4983-9

Gizon L, Birch AC (2005) Local Helioseismology. Living Reviews in Solar Physics 2(1):6. https://doi.org/10.12942/lrsp-2005-6

Gizon L, Birch AC (2012) Helioseismology challenges models of solar convection. Proceedings of the National Academy of Sciences 109(30):11,896–11,897. https://doi.org/10.1073/pnas.1208875109

Gizon L, Duvall TL, Schou J (2003) Wave-like properties of solar supergranulation. Nature421(6918):43–44. https://doi.org/10.1038/nature01287, https://arxiv.org/abs/arXiv:astro-ph/0208343 [astro-ph]

Gizon L, Cameron RH, Pourabdian M, et al (2020a) Meridional flow in the Sun's convection zone is a single cell in each hemisphere. Science 368(6498):1469–1472. https://doi.org/10.1126/science.aaz7119

Gizon L, Fournier D, Albekioni M (2020b) Effect of latitudinal differential rotation on solar Rossby waves: Critical layers, eigenfunctions, and momentum fluxes in the equatorial $\beta$ plane. A&A642:A178. https://doi.org/10.1051/0004-6361/202038525, https://arxiv.org/abs/arXiv:2008.02185 [astro-ph.SR]

Gizon L, Cameron RH, Bekki Y, et al (2021) Solar inertial modes: Observations, identification, and diagnostic promise. A&A652:L6. https://doi.org/10.1051/0004-6361/202141462, https://arxiv.org/abs/arXiv:2107.09499 [astro-ph.SR]

Glatzmaier GA (1984) Numerical simulations of stellar convective dynamos. I. the model and method. Journal of Computational Physics 55(3):461–484. https://doi.org/10.1016/0021-9991(84)90033-0

Glatzmaier GA (1985) Numerical simulations of stellar convective dynamos. II - Field propagation in the convection zone. ApJ291:300–307. https://doi.org/10.1086/163069

Glatzmaier GA, Gilman PA (1981) Compressible Convection in a Rotating Spherical Shell - Part Three - Analytic Model for Compressible Vorticity Waves. ApJS45:381. https://doi.org/10.1086/190716

Glatzmaier GA, Gilman PA (1982) Compressible convection in a rotating spherical shell. V - Induced differential rotation and meridional circulation. ApJ256:316–330. https://doi.org/10.1086/159909

Goldbaum N, Rast MP, Ermolli I, et al (2009) The Intensity Profile of the Solar Supergranulation. ApJ707(1):67–73. https://doi.org/10.1088/0004-637X/707/1/67, https://arxiv.org/abs/arXiv:0909.3310 [astro-ph.SR]

González Hernández I, Kholikov S, Hill F, et al (2008) Subsurface Meridional Circulation in the Active Belts. Sol. Phys.252(2):235–245. https://doi.org/10.1007/s11207-008-9264-y, https://arxiv.org/abs/arXiv:0808.3606 [astro-ph]

Gough DO (1969) The Anelastic Approximation for Thermal Convection. Journal of Atmospheric Sciences 26(3):448–456. https://doi.org/10.1175/1520-0469(1969)026⟨0448:TAAFTC⟩2.0.CO;2

Greenspan H, Batchelor C, Ablowitz M, et al (1968) The Theory of Rotating Fluids. Cambridge Monographs on Mechanics, Cambridge University Press, URL https://books.google.de/books?id=2R47AAAAIAAJ

Greer BJ, Hindman BW, Featherstone NA, et al (2015) Helioseismic Imaging of Fast Convective Flows throughout the Near-surface Shear Layer. ApJ803(2):L17. https://doi.org/10.1088/2041-8205/803/2/L17, https://arxiv.org/abs/arXiv:1504.00699 [astro-ph.SR]

Guerrero G, Smolarkiewicz PK, Kosovichev AG, et al (2013) Differential rotation in solar-like stars from global simulations. The Astrophysical Journal 779:176. https://doi.org/10.1088/0004-637X/779/2/176

Haber DA, Hindman BW, Toomre J, et al (2002) Evolving Submerged Meridional Circulation Cells within the Upper Convection Zone Revealed by Ring-Diagram Analysis. ApJ570(2):855–864. https://doi.org/10.1086/339631

Hanasoge SM (2022) Surface and interior meridional circulation in the Sun. Living Reviews in Solar Physics 19(1):3. https://doi.org/10.1007/s41116-022-00034-7

Hanasoge SM, Duvall TL, Sreenivasan KR (2012) Anomalously weak solar convection. Proceedings of the National Academy of Science 109(30):11,928–11,932. https://doi.org/10.1073/pnas.1206570109, https://arxiv.org/abs/arXiv:1206.3173 [astro-ph.SR]

Hanson CS, Gizon L, Liang ZC (2020) Solar Rossby waves observed in GONG++ ring-diagram flow maps. A&A635:A109. https://doi.org/10.1051/0004-6361/201937321, https://arxiv.org/abs/arXiv:2002.01194 [astro-ph.SR]

Hanson CS, Hanasoge S, Sreenivasan KR (2022) Discovery of high-frequency retrograde vorticity waves in the Sun. Nature Astronomy 6:708–714. https://doi.org/10.1038/s41550-022-01632-z

Hart AB (1954) Motions in the Sun at the photospheric level. IV. The equatorial rotation and possible velocity fields in the photosphere. MNRAS114:17. https://doi.org/10.1093/mnras/114.1.17

Hathaway DH (1996) Doppler Measurements of the Sun's Meridional Flow. ApJ460:1027. https://doi.org/10.1086/177029

Hathaway DH, Rightmire L (2010) Variations in the Sun's Meridional Flow over a Solar Cycle. Science 327(5971):1350. https://doi.org/10.1126/science.1181990

Hathaway DH, Upton LA (2021) Hydrodynamic Properties of the Sun's Giant Cellular Flows. ApJ908(2):160. https://doi.org/10.3847/1538-4357/abcbfa, https://arxiv.org/abs/arXiv:2006.06084 [astro-ph.SR]

Hathaway DH, Beck JG, Bogart RS, et al (2000) The Photospheric Convection Spectrum. Sol. Phys.193:299–312. https://doi.org/10.1023/A:1005200809766

Hathaway DH, Upton L, Colegrove O (2013) Giant Convection Cells Found on the Sun. Science 342(6163):1217–1219. https://doi.org/10.1126/science.1244682

Hathaway DH, Teil T, Norton AA, et al (2015) The Sun's Photospheric Convection Spectrum. ApJ811(2):105. https://doi.org/10.1088/0004-637X/811/2/105, https://arxiv.org/abs/arXiv:1508.03022 [astro-ph.SR]

Hazra G, Karak BB, Choudhuri AR (2014) Is a Deep One-cell Meridional Circulation Essential for the Flux Transport Solar Dynamo? ApJ782(2):93. https://doi.org/10.1088/0004-637X/782/2/93, https://arxiv.org/abs/arXiv:1309.2838 [astro-ph.SR]

Heimpel M, Gastine T, Wicht J (2016) Simulation of deep-seated zonal jets and shallow vortices in gas giant atmospheres. Nature Geoscience 9(1):19–23. https://doi.org/10.1038/ngeo2601

Henry GW, Eaton JA, Hamer J, et al (1995) Starspot Evolution, Differential Rotation, and Magnetic Cycles in the Chromospherically Active Binaries lambda Andromedae, sigma Geminorum, II Pegasi, and V711 Tauri. ApJS97:513. https://doi.org/10.1086/192149

Herschel W (1801) Observations Tending to Investigate the Nature of the Sun, in Order to Find the Causes or Symptoms of Its Variable Emission of Light and Heat; With Remarks on the Use That May Possibly Be Drawn from Solar Observations. Philosophical Transactions of the Royal Society of London Series I 91:265–318

Hindman BW, Jain R (2022) Radial Trapping of Thermal Rossby Waves within the Convection Zones of Low-mass Stars. ApJ932(1):68. https://doi.org/10.3847/1538-4357/ac6d64, https://arxiv.org/abs/arXiv:2205.02346 [astro-ph.SR]

Hindman BW, Featherstone NA, Julien K (2020) Morphological Classification of the Convective Regimes in Rotating Stars. The Astrophysical Journal 898(2):120. https://doi.org/10.3847/1538-4357/ab9ec2

Hirzberger J (2002) On the brightness and velocity structure of solar granulation. A&A392:1105–1118. https://doi.org/10.1051/0004-6361:20020902

Hotta H (2017) Solar Overshoot Region and Small-scale Dynamo with Realistic Energy Flux. ApJ843(1):52. https://doi.org/10.3847/1538-4357/aa784b, https://arxiv.org/abs/arXiv:1706.06413 [astro-ph.SR]

Hotta H (2018) Breaking Taylor-Proudman Balance by Magnetic Fields in Stellar Convection Zones. ApJ860(2):L24. https://doi.org/10.3847/2041-8213/aacafb, https://arxiv.org/abs/arXiv:1806.01452 [astro-ph.SR]

Hotta H, Kusano K (2021) Solar differential rotation reproduced with high-resolution simulation. Nature Astronomy 5:1100–1102. https://doi.org/10.1038/s41550-021-01459-0, https://arxiv.org/abs/arXiv:2109.06280 [astro-ph.SR]

Hotta H, Rempel M, Yokoyama T, et al (2012) Numerical calculation of convection with reduced speed of sound technique. A&A539:A30. https://doi.org/10.1051/0004-6361/201118268, https://arxiv.org/abs/arXiv:1201.1061 [astro-ph.SR]

Hotta H, Rempel M, Yokoyama T (2015a) Efficient Small-scale Dynamo in the Solar Convection Zone. ApJ803(1):42. https://doi.org/10.1088/0004-637X/803/1/42, https://arxiv.org/abs/arXiv:1502.03846 [astro-ph.SR]

Hotta H, Rempel M, Yokoyama T (2015b) High-resolution Calculation of the Solar Global Convection with the Reduced Speed of Sound Technique. II. Near Surface Shear Layer with the Rotation. ApJ798(1):51. https://doi.org/10.1088/0004-637X/798/1/51, https://arxiv.org/abs/arXiv:1410.7093 [astro-ph.SR]

Hotta H, Rempel M, Yokoyama T (2016) Large-scale magnetic fields at high Reynolds numbers in magnetohydrodynamic simulations. Science 351(6280):1427–1430. https://doi.org/10.1126/science.aad1893

Hotta H, Iijima H, Kusano K (2019) Weak influence of near-surface layer on solar deep convection zone revealed by comprehensive simulation from base to surface. Science Advances 5(1):2307. https://doi.org/10.1126/sciadv.aau2307

Hotta H, Kusano K, Shimada R (2022) Generation of Solar-like Differential Rotation. ApJ933(2):199. https://doi.org/10.3847/1538-4357/ac7395, https://arxiv.org/abs/arXiv:2202.04183 [astro-ph.SR]

Howe R, Christensen-Dalsgaard J, Hill F, et al (2000) Dynamic Variations at the Base of the Solar Convection Zone. Science 287(5462):2456–2460. https://doi.org/10.1126/science.287.5462.2456

Howe R, Christensen-Dalsgaard J, Hill F, et al (2005) Solar Convection-Zone Dynamics, 1995-2004. ApJ634(2):1405–1415. https://doi.org/10.1086/

497107

Jackiewicz J, Serebryanskiy A, Kholikov S (2015) Meridional Flow in the Solar Convection Zone. II. Helioseismic Inversions of GONG Data. ApJ805(2):133. https://doi.org/10.1088/0004-637X/805/2/133, https://arxiv.org/abs/arXiv:1504.08071 [astro-ph.SR]

Käpylä PJ (2019) Overshooting in simulations of compressible convection. A&A631:A122. https://doi.org/10.1051/0004-6361/201834921, https://arxiv.org/abs/arXiv:1812.07916 [astro-ph.SR]

Käpylä PJ, Mantere MJ, Guerrero G, et al (2011) Reynolds stress and heat flux in spherical shell convection. A&A531:A162. https://doi.org/10.1051/0004-6361/201015884, https://arxiv.org/abs/arXiv:1010.1250 [astro-ph.SR]

Karak BB, Käpylä PJ, Käpylä MJ, et al (2015) Magnetically controlled stellar differential rotation near the transition from solar to anti-solar profiles. Astronomy & Astrophysics 576:A26. https://doi.org/10.1051/0004-6361/201424521

Karak BB, Miesch M, Bekki Y (2018) Consequences of high effective Prandtl number on solar differential rotation and convective velocity. Physics of Fluids 30(4):046,602. https://doi.org/10.1063/1.5022034, https://arxiv.org/abs/arXiv:1801.00560

Karoff C, Metcalfe TS, Santos ARG, et al (2018) The Influence of Metallicity on Stellar Differential Rotation and Magnetic Activity. The Astrophysical Journal 852(1):46. https://doi.org/10.3847/1538-4357/aaa026

Kueker M, Ruediger G (2011) Differential rotation and meridional flow on the lower zero age main sequence: Reynolds stress versus baroclinic flow. Astronomische Nachrichten 332(9-10):933–938. https://doi.org/10.1002/asna.201111628, https://arxiv.org/abs/arXiv:1110.4757

Käpylä PJ, Käpylä MJ, Brandenburg A (2014) Confirmation of bistable stellar differential rotation profiles. Astronomy & Astrophysics 570:A43. https://doi.org/10.1051/0004-6361/201423412

Langfellner J, Birch AC, Gizon L (2018) Evolution and wave-like properties of the average solar supergranule. A&A617:A97. https://doi.org/10.1051/0004-6361/201732471, https://arxiv.org/abs/arXiv:1805.12522 [astro-ph.SR]

Lantz SR (1992) Dynamical Behavior of Magnetic Fields in a Stratified, Convecting Fluid Layer. PhD thesis, Cornell University, New York

Larson TP, Schou J (2018) Global-Mode Analysis of Full-Disk Data from the Michelson Doppler Imager and the Helioseismic and Magnetic Imager. Sol. Phys.293(2):29. https://doi.org/10.1007/s11207-017-1201-5

Leighton RB, Noyes RW, Simon GW (1962) Velocity Fields in the Solar Atmosphere. I. Preliminary Report. ApJ135:474. https://doi.org/10.1086/147285

Leitzinger M, Brandt PN, Hanslmeier A, et al (2005) Dynamics of solar mesogranulation. A&A444(1):245–255. https://doi.org/10.1051/0004-6361:20053152

Liang ZC, Chou DY (2015) Effects of Solar Surface Magnetic Fields on the Time-Distance Analysis of Solar Subsurface Meridional Flows. ApJ805(2):165. https://doi.org/10.1088/0004-637X/805/2/165

Liang ZC, Birch AC, Duvall JThomas L., et al (2017) Comparison of acoustic travel-time measurements of solar meridional circulation from SDO/HMI and SOHO/MDI. A&A601:A46. https://doi.org/10.1051/0004-6361/201730416, https://arxiv.org/abs/arXiv:1704.00475 [astro-ph.SR]

Liang ZC, Gizon L, Birch AC, et al (2018) Solar meridional circulation from twenty-one years of SOHO/MDI and SDO/HMI observations. Helioseismic travel times and forward modeling in the ray approximation. A&A619:A99. https://doi.org/10.1051/0004-6361/201833673, https://arxiv.org/abs/arXiv:1808.08874 [astro-ph.SR]

Liang ZC, Gizon L, Birch AC, et al (2019) Time-distance helioseismology of solar Rossby waves. A&A626:A3. https://doi.org/10.1051/0004-6361/201834849, https://arxiv.org/abs/arXiv:1812.07413 [astro-ph.SR]

Lisle JP, Rast MP, Toomre J (2004) Persistent North-South Alignment of the Solar Supergranulation. ApJ608(2):1167–1174. https://doi.org/10.1086/420691

Löptien B, Gizon L, Birch AC, et al (2018) Global-scale equatorial Rossby waves as an essential component of solar internal dynamics. Nature Astronomy 2:568–573. https://doi.org/10.1038/s41550-018-0460-x, https://arxiv.org/abs/arXiv:1805.07244 [astro-ph.SR]

Lord JW (2014) Deep Convection, Magnetism and Solar Supergranulation. PhD thesis, University of Colorado at Boulder

Lord JW, Cameron RH, Rast MP, et al (2014) The Role of Subsurface Flows in Solar Surface Convection: Modeling the Spectrum of Supergranular and Larger Scale Flows. ApJ793(1):24. https://doi.org/10.1088/0004-637X/

793/1/24, https://arxiv.org/abs/arXiv:1407.2209 [astro-ph.SR]

Mandal K, Hanasoge S (2020) Properties of Solar Rossby Waves from Normal Mode Coupling and Characterizing Its Systematics. ApJ891(2):125. https://doi.org/10.3847/1538-4357/ab7227, https://arxiv.org/abs/arXiv:1908.05890 [astro-ph.SR]

Mandal K, Hanasoge SM, Rajaguru SP, et al (2018) Helioseismic Inversion to Infer the Depth Profile of Solar Meridional Flow Using Spherical Born Kernels. ApJ863(1):39. https://doi.org/10.3847/1538-4357/aacea2, https://arxiv.org/abs/arXiv:1807.00314 [astro-ph.SR]

Matilsky LI, Hindman BW, Toomre J (2019) The Role of Downflows in Establishing Solar Near-surface Shear. ApJ871(2):217. https://doi.org/10.3847/1538-4357/aaf647, https://arxiv.org/abs/arXiv:1810.00115 [astro-ph.SR]

Matilsky LI, Hindman BW, Toomre J (2020) Revisiting the Sun's Strong Differential Rotation along Radial Lines. ApJ898(2):111. https://doi.org/10.3847/1538-4357/ab9ca0, https://arxiv.org/abs/arXiv:2004.00208 [astro-ph.SR]

Matt S, Do Cao O, Brown B, et al (2011) Convection and differential rotation properties of G and K stars computed with the ASH code. Astronomische Nachrichten 332(9-10):897–906. https://doi.org/10.1002/asna.201111624

McIntyre ME (1999) Breaking Waves and Global-Scale Chemical Transport in the Earth's Atmosphere, with Spinoffs for the Sun's Interior. Progress of Theoretical Physics 101(1):189–189. https://doi.org/10.1143/PTP.101.189

Metcalfe TS, Finley AJ, Kochukhov O, et al (2022) The Origin of Weakened Magnetic Braking in Old Solar Analogs. The Astrophysical Journal Letters 933(1):L17. https://doi.org/10.3847/2041-8213/ac794d

Miesch MS (2005) Large-Scale Dynamics of the Convection Zone and Tachocline. Living Reviews in Solar Physics 2:1. https://doi.org/10.12942/lrsp-2005-1

Miesch MS, Hindman BW (2011) Gyroscopic Pumping in the Solar Near-surface Shear Layer. ApJ743(1):79. https://doi.org/10.1088/0004-637X/743/1/79, https://arxiv.org/abs/arXiv:1106.4107 [astro-ph.SR]

Miesch MS, Elliott JR, Toomre J, et al (2000) Three-dimensional Spherical Simulations of Solar Convection. I. Differential Rotation and Pattern Evolution Achieved with Laminar and Turbulent States. ApJ532(1):593–615. https://doi.org/10.1086/308555

Miesch MS, Brun AS, Toomre J (2006) Solar Differential Rotation Influenced by Latitudinal Entropy Variations in the Tachocline. The Astrophysical Journal 641(1):618–625. https://doi.org/10.1086/499621

Miesch MS, Brun AS, DeRosa ML, et al (2008) Structure and Evolution of Giant Cells in Global Models of Solar Convection. ApJ673(1):557–575. https://doi.org/10.1086/523838, https://arxiv.org/abs/arXiv:0707.1460 [astro-ph]

Mori K, Hotta H (2023) Investigation of the dependence of angular momentum transport on spatial scales for construction of differential rotation. MNRAS519(2):3091–3097. https://doi.org/10.1093/mnras/stac3804, https://arxiv.org/abs/arXiv:2212.11502 [astro-ph.SR]

Muñoz-Jaramillo A, Nandy D, Martens PCH (2011) Magnetic Quenching of Turbulent Diffusivity: Reconciling Mixing-length Theory Estimates with Kinematic Dynamo Models of the Solar Cycle. ApJ727(1):L23. https://doi.org/10.1088/2041-8205/727/1/L23, https://arxiv.org/abs/arXiv:1007.1262 [astro-ph.SR]

Nagashima K, Zhao J, Kosovichev AG, et al (2011) Detection of Supergranulation Alignment in Polar Regions of the Sun by Helioseismology. ApJ726(2):L17. https://doi.org/10.1088/2041-8205/726/2/L17, https://arxiv.org/abs/arXiv:1011.1025 [astro-ph.SR]

Nagashima K, Birch AC, Schou J, et al (2020) An improved multi-ridge fitting method for ring-diagram helioseismic analysis. A&A633:A109. https://doi.org/10.1051/0004-6361/201936662, https://arxiv.org/abs/arXiv:1911.07772 [astro-ph.SR]

Nelson NJ, Brown BP, Brun AS, et al (2013) Magnetic Wreaths and Cycles in Convective Dynamos. ApJ762(2):73. https://doi.org/10.1088/0004-637X/762/2/73, https://arxiv.org/abs/arXiv:1211.3129 [astro-ph.SR]

Nesis A, Hanslmeier A, Hammer R, et al (1992) Dynamics of the solar granulation. I - A phenomenological approach. A&A253(2):561–566

Noraz Q (2022) Magnétisme et dynamique des étoiles de type solaire. PhD thesis, Université Paris-Cité

Noraz Q, Breton SN, Brun AS, et al (2022a) Hunting for anti-solar differentially rotating stars using the Rossby number: An application to the *Kepler* field. Astronomy & Astrophysics 667:A50. https://doi.org/10.1051/0004-6361/202243890

Noraz Q, Brun AS, Strugarek A, et al (2022b) Impact of anti-solar differential rotation in mean-field solar-type dynamos: Exploring possible magnetic

cycles in slowly rotating stars. Astronomy & Astrophysics 658:A144. https://doi.org/10.1051/0004-6361/202141946

Nordlund Å, Stein RF, Asplund M (2009) Solar Surface Convection. Living Reviews in Solar Physics 6(1):2. https://doi.org/10.12942/lrsp-2009-2

November LJ, Toomre J, Gebbie KB, et al (1981) The detection of mesogranulation on the Sun. ApJ245:L123–L126. https://doi.org/10.1086/183539

O'Mara B, Miesch MS, Featherstone NA, et al (2016) Velocity amplitudes in global convection simulations: The role of the Prandtl number and near-surface driving. Advances in Space Research 58(8):1475–1489. https://doi.org/10.1016/j.asr.2016.03.038, https://arxiv.org/abs/arXiv:1603.06107 [astro-ph.SR]

Ortiz A, Rast M (2005) How good is the Ca II K as a proxy for the magnetic flux? Mem. Soc. Astron. Italiana76:1018

Papaloizou J, Pringle JE (1978) Non-radial oscillations of rotating stars and their relevance to the short-period oscillations of cataclysmic variables. MNRAS182:423–442. https://doi.org/10.1093/mnras/182.3.423

Patron J, Hill F, Rhodes JE. J., et al (1995) Velocity Fields within the Solar Convection Zone: Evidence from Oscillation Ring Diagram Analysis of Mount Wilson Dopplergrams. ApJ455:746. https://doi.org/10.1086/176620

Philidet J, Gizon L (2023) Interaction of solar inertial modes with turbulent convection. A 2D model for the excitation of linearly stable modes. A&A673:A124. https://doi.org/10.1051/0004-6361/202245666, https://arxiv.org/abs/arXiv:2304.05926 [astro-ph.SR]

Proxauf B (2020) Observations of large-scale solar flows. PhD thesis, Georg August University of Gottingen, Germany

Proxauf B, Gizon L, Löptien B, et al (2020) Exploring the latitude and depth dependence of solar Rossby waves using ring-diagram analysis. A&A634:A44. https://doi.org/10.1051/0004-6361/201937007, https://arxiv.org/abs/arXiv:1912.02056 [astro-ph.SR]

Rajaguru SP, Antia HM (2015) Meridional Circulation in the Solar Convection Zone: Time-Distance Helioseismic Inferences from Four Years of HMI/SDO Observations. ApJ813(2):114. https://doi.org/10.1088/0004-637X/813/2/114, https://arxiv.org/abs/arXiv:1510.01843 [astro-ph.SR]

Rast MP (1995) On the Nature of "Exploding" Granules and Granule Fragmentation. ApJ443:863. https://doi.org/10.1086/175576

Rast MP (2003) The Scales of Granulation, Mesogranulation, and Supergranulation. ApJ597(2):1200–1210. https://doi.org/10.1086/381221

Rast MP (2020) Deciphering Solar Convection. In: Monteiro MJPFG, García RA, Christensen-Dalsgaard J, et al (eds) Dynamics of the Sun and Stars; Honoring the Life and Work of Michael J. Thompson, pp 149–161, https://doi.org/10.1007/978-3-030-55336-4_23

Rast MP, Toomre J (1993) Compressible Convection with Ionization. I. Stability, Flow Asymmetries, and Energy Transport. ApJ419:224. https://doi.org/10.1086/173477

Rauer H, Catala C, Aerts C, et al (2014) The PLATO 2.0 mission. Experimental Astronomy 38(1-2):249–330. https://doi.org/10.1007/s10686-014-9383-4

Reiners A (2007) Differential rotation in F stars. Astronomische Nachrichten 328(10):1034–1036. https://doi.org/10.1002/asna.200710853

Reiners A, Schmitt JHMM (2003) Rotation and differential rotation in field F- and G-type stars. Astronomy & Astrophysics 398(2):647–661. https://doi.org/10.1051/0004-6361:20021642

Reinhold T, Arlt R (2015) Discriminating solar and antisolar differential rotation in high-precision light curves. Astronomy & Astrophysics 576:A15. https://doi.org/10.1051/0004-6361/201425337

Reinhold T, Gizon L (2015) Rotation, differential rotation, and gyrochronology of active *Kepler* stars. Astronomy & Astrophysics 583:A65. https://doi.org/10.1051/0004-6361/201526216

Reinhold T, Reiners A, Basri G (2013) Rotation and differential rotation of active *Kepler* stars. Astronomy & Astrophysics 560:A4. https://doi.org/10.1051/0004-6361/201321970

Rempel M (2005) Solar Differential Rotation and Meridional Flow: The Role of a Subadiabatic Tachocline for the Taylor-Proudman Balance. ApJ622(2):1320–1332. https://doi.org/10.1086/428282, https://arxiv.org/abs/arXiv:astro-ph/0604451 [astro-ph]

Rhines PB (1975) Waves and turbulence on a beta-plane. Journal of Fluid Mechanics 69(3):417–443. https://doi.org/10.1017/S0022112075001504

Rieutord M, Rincon F (2010) The Sun's Supergranulation. Living Reviews in Solar Physics 7(1):2. https://doi.org/10.12942/lrsp-2010-2, https://arxiv.org/abs/arXiv:1005.5376 [astro-ph.SR]

Rieutord M, Roudier T, Malherbe JM, et al (2000) On mesogranulation, network formation and supergranulation. A&A357:1063–1072

Rincon F, Rieutord M (2018) The Sun's supergranulation. Living Reviews in Solar Physics 15(1):6. https://doi.org/10.1007/s41116-018-0013-5

Roberts PH (1968) On the Thermal Instability of a Rotating-Fluid Sphere Containing Heat Sources. Philosophical Transactions of the Royal Society of London Series A 263(1136):93–117. https://doi.org/10.1098/rsta.1968.0007

Saar SH (2010) Starspots, cycles, and magnetic fields. Proceedings of the International Astronomical Union 6(S273):61–67. https://doi.org/10.1017/S1743921311015018

Saio H (1982) R-mode oscillations in uniformly rotating stars. ApJ256:717–735. https://doi.org/10.1086/159945

Schou J (2003) Wavelike Properties of Solar Supergranulation Detected in Doppler Shift Data. ApJ596(2):L259–L262. https://doi.org/10.1086/379529

Schou J, Antia HM, Basu S, et al (1998) Helioseismic Studies of Differential Rotation in the Solar Envelope by the Solar Oscillations Investigation Using the Michelson Doppler Imager. ApJ505(1):390–417. https://doi.org/10.1086/306146

See V, Roquette J, Amard L, et al (2021) Photometric variability as a proxy for magnetic activity and its dependence on metallicity. arXiv:210305675 [astro-ph] https://arxiv.org/abs/arXiv:2103.05675 [astro-ph]

Simitev RD, Kosovichev AG, Busse FH (2015) Dynamo effects near the transition from solar to anti-solar differential rotation. The Astrophysical Journal 810(1):80. https://doi.org/10.1088/0004-637X/810/1/80

Simon GW, Leighton RB (1964) Velocity Fields in the Solar Atmosphere. III. Large-Scale Motions, the Chromospheric Network, and Magnetic Fields. ApJ140:1120. https://doi.org/10.1086/148010

Simon GW, Weiss NO (1968) Supergranules and the Hydrogen Convection Zone. ZAp69:435

Skumanich A (1972) Time scales for ca ii emission decay, rotational braking, and lithium depletion. ApJ p 4

Spruit HC (1997) Convection in stellar envelopes: a changing paradigm. Mem. Soc. Astron. Italiana68:397–413. https://arxiv.org/abs/arXiv:astro-ph/9605020 [astro-ph]

Stein RF, Georgobiani D, Schafenberger W, et al (2009) Supergranulation Scale Convection Simulations. In: Stempels E (ed) 15th Cambridge Workshop on Cool Stars, Stellar Systems, and the Sun, pp 764–767, https://doi.org/10.1063/1.3099227

Stejko AM, Kosovichev AG, Pipin VV (2021) Forward Modeling Helioseismic Signatures of One- and Two-cell Meridional Circulation. ApJ911(2):90. https://doi.org/10.3847/1538-4357/abec70, https://arxiv.org/abs/arXiv:2101.01220 [astro-ph.SR]

Stix M (2002) The sun: an introduction. Springer Berlin Heidelberg

Thibault K, Charbonneau P, Crouch AD (2012) The Buildup of a Scale-free Photospheric Magnetic Network. ApJ757(2):187. https://doi.org/10.1088/0004-637X/757/2/187

Thompson MJ, Toomre J, Anderson ER, et al (1996) Differential Rotation and Dynamics of the Solar Interior. Science 272(5266):1300–1305. https://doi.org/10.1126/science.272.5266.1300

Triana SA, Guerrero G, Barik A, et al (2022) Identification of Inertial Modes in the Solar Convection Zone. ApJ934(1):L4. https://doi.org/10.3847/2041-8213/ac7dac, https://arxiv.org/abs/arXiv:2204.13007 [astro-ph.SR]

Ulrich RK (2010) Solar Meridional Circulation from Doppler Shifts of the Fe I Line at 5250 Å as Measured by the 150-foot Solar Tower Telescope at the Mt. Wilson Observatory. ApJ725(1):658–669. https://doi.org/10.1088/0004-637X/725/1/658, https://arxiv.org/abs/arXiv:1010.0487 [astro-ph.SR]

Unno W, Osaki Y, Ando H, et al (1989) Nonradial oscillations of stars

van Ballegooijen AA (1986) On the Surface Response of Solar Giant Cells. ApJ304:828. https://doi.org/10.1086/164219

Vasil GM, Lecoanet D, Brown BP, et al (2013) Energy conservation and gravity waves in sound-proof treatments of stellar interiors. II. Lagrangian constrained analysis. The Astrophysical Journal 773(2):169. https://doi.org/10.1088/0004-637X/773/2/169

Vasil GM, Julien K, Featherstone NA (2021) Rotation suppresses giant-scale solar convection. Proceedings of the National Academy of Science 118(31):e2022518118. https://doi.org/10.1073/pnas.2022518118

Viviani M, Käpylä MJ, Warnecke J, et al (2019) Stellar Dynamos in the Transition Regime: Multiple Dynamo Modes and Antisolar Differential Rotation. The Astrophysical Journal 886(1):21. https://doi.org/10.3847/1538-4357/

ab3e07

Warnecke J (2018) Dynamo cycles in global convection simulations of solar-like stars. Astronomy & Astrophysics 616:A72. https://doi.org/10.1051/0004-6361/201732413

Witzke V, Duehnen HB, Shapiro AI, et al (2022) Small-scale dynamo in cool main sequence stars. II. The effect of metallicity. 2211.02722

Yadav RK, Christensen UR, Morin J, et al (2015) Explaining the coexistence of large-scale and small-scale magnetic fields in fully convective stars. The Astrophysical Journal 813(2):L31. https://doi.org/10.1088/2041-8205/813/2/L31

Zhao J, Nagashima K, Bogart RS, et al (2012) Systematic Center-to-limb Variation in Measured Helioseismic Travel Times and its Effect on Inferences of Solar Interior Meridional Flows. ApJ749(1):L5. https://doi.org/10.1088/2041-8205/749/1/L5, https://arxiv.org/abs/arXiv:1203.1904 [astro-ph.SR]

Zhao J, Bogart RS, Kosovichev AG, et al (2013) Detection of Equatorward Meridional Flow and Evidence of Double-cell Meridional Circulation inside the Sun. ApJ774(2):L29. https://doi.org/10.1088/2041-8205/774/2/L29, https://arxiv.org/abs/arXiv:1307.8422 [astro-ph.SR]